AMERICAN SOCIETY FOR MICROBIOLOGY | Journal of Virology®

STRUCTURE AND ASSEMBLY

Conformational Engineering of HIV-1 Env Based on Mutational Tolerance in the CD4 and PG16 Bound States

Jeremiah D. Heredia,[a] Jihye Park,[a] Hannah Choi,[a] Kevin S. Gill,[a] Erik Procko[a]

[a]Department of Biochemistry, University of Illinois at Urbana-Champaign, Urbana, Illinois, USA

ABSTRACT HIV-1 infection is initiated by viral Env engaging the host receptor CD4, triggering Env to transition from a "closed" to "open" conformation during the early events of virus-cell membrane fusion. To understand how Env sequence accommodates this conformational change, mutational landscapes decoupled from virus replication were determined for Env from BaL (clade B) and DU422 (clade C) isolates interacting with CD4 or antibody PG16 that preferentially recognizes closed trimers. Sequence features uniquely important to each bound state were identified, including glycosylation and binding sites. Notably, the Env apical domain and trimerization interface are under selective pressure for PG16 binding. Based on this key observation, mutations were found that increase presentation of quaternary epitopes associated with properly conformed trimers when Env is expressed at the plasma membrane. Many mutations reduce electrostatic repulsion at the Env apex and increase PG16 recognition of Env sequences from clades A and B. Other mutations increase hydrophobic packing at the gp120 inner-outer domain interface and were broadly applicable for engineering Env from diverse strains spanning tiers 1, 2, and 3 across clades A, B, C, and BC recombinants. Core mutations predicted to introduce steric strain in the open state show markedly reduced CD4 interactions. Finally, we demonstrate how our methodology can be adapted to interrogate interactions between membrane-associated Env and the matrix domain of Gag. These findings and methods may assist vaccine design.

IMPORTANCE HIV-1 Env is dynamic and undergoes large conformational changes that drive fusion of virus and host cell membranes. Three Env proteins in a trimer contact each other at their apical tips to form a closed conformation that presents epitopes recognized by broadly neutralizing antibodies. The apical tips separate, among other changes, to form an open conformation that binds tightly to host receptors. Understanding how Env sequence facilitates these structural changes can inform the biophysical mechanism and aid immunogen design. Using deep mutational scans decoupled from virus replication, we report mutational landscapes for Env from two strains interacting with conformation-dependent binding proteins. Residues in the Env trimer interface and apical domains are preferentially conserved in the closed conformation, and conformational diversity is facilitated by electrostatic repulsion and an underpacked core between domains. Specific mutations are described that enhance presentation of the trimeric closed conformation across diverse HIV-1 strains.

KEYWORDS CD4, Env, broadly neutralizing antibody, conformational change, deep mutational scan, directed evolution, gp160, human immunodeficiency virus, protein engineering, quaternary epitope

HIV-1 engages target cells through interactions between the viral glycoprotein Env and host receptors. HIV-1 Env is formed by a homotrimeric complex of gp160 subunits that are cleaved by host proteases during maturation into extracellular gp120

Citation Heredia JD, Park J, Choi H, Gill KS, Procko E. 2019. Conformational engineering of HIV-1 Env based on mutational tolerance in the CD4 and PG16 bound states. J Virol 93:e00219-19. https://doi.org/10.1128/JVI.00219-19.

Editor Frank Kirchhoff, Ulm University Medical Center

Copyright © 2019 American Society for Microbiology. All Rights Reserved.

Address correspondence to Erik Procko, procko@illinois.edu.

Received 7 February 2019
Accepted 16 March 2019
Accepted manuscript posted online 20 March 2019
Published 15 May 2019

Downloaded from https://journals.asm.org/journal/jvi on 24 February 2022 by 65.21.193.86.

and membrane-tethered gp41, which remain noncovalently associated in a "closed" conformation that can dynamically sample alternative conformational states (1). During infection, the gp120 subunit binds the primary host receptor CD4, inducing an "open" conformation of Env that exposes binding sites for a secondary coreceptor (2–4). This coreceptor is one of either two chemokine receptors, CCR5 or CXCR4, and once bound, further conformational changes release fusogenic regions of gp41 that mediate membrane fusion and viral entry into the host cell.

Env is the only viral protein on the outside of an HIV-1 virion accessible to the humoral immune system, and it therefore has been extensively studied for vaccine development (5). Conformational diversity that causes exposure of nonneutralizing or strain-specific immunodominant epitopes (6–10), Env sequence diversity, and epitope shielding by extensive glycosylation all act to limit potency and breadth of the host response. Many broadly neutralizing antibodies (bNAbs) recognize Env in the closed state, but the design and purification of Env immunogens that correctly fold into native-like, prefusion closed trimers is challenging due to intrinsic conformational flexibility (11, 12). A widely used construct for purifying the extracellular region of Env as a soluble trimer, called SOSIP, incorporates a disulfide between gp41 and gp120 subunits, and an I559P substitution to destabilize the postfusion state (13–15). SOSIP constructs from various strains have been heavily engineered with additional mutations for favorable antigenic profiles, trimer stability, purification properties, structure, and reduced exposure of strain-specific V3 and CD4i epitopes (16–18). Closed SOSIP trimers can be isolated with high purity using conformation specific antibodies, but for full-length or close to full-length Env that is membrane anchored, appropriately folded protein cannot be easily separated from misfolded forms. This means that nucleic acid vaccines or virus-like particles (VLPs) can present a heterogeneous mixture of full-length Env in monomeric, oligomeric, closed, open, and partially open conformers. While VLPs can be treated with protease to remove sensitive misfolded forms (19), there would ideally exist sequence variants of Env that are primarily expressed as closed trimers. Understanding how Env sequence dictates conformation therefore not only addresses important biophysical questions on how protein dynamics are governed by primary structure but may also assist the design of sophisticated Env immunogens.

Deep mutational scanning couples directed evolution of diverse sequence populations with next-generation sequencing to track the phenotypic fitness of thousands of mutations simultaneously (20). The method has been used for vaccine design to screen for mutations within extracellular Env constructs that enhance direct interactions with an antibody and its germ line precursors, reduce exposure of V3 epitopes, and improve SOSIP thermostability (17, 21, 22); however, none of these data sets have been analyzed to address the central question behind this study; how does Env sequence relate to conformational change? Tissue culture propagation experiments of viruses expressing Env variants have also been extensively followed by next-generation sequencing and have shown that a surprisingly small number among the thousands of possible mutations in Env are positively selected for escape from antibody neutralization (23, 24). However, virus propagation demands that Env fold, traffic to the cell surface, incorporate into a budding virion, bind target receptors, and catalyze membrane fusion, and these mutational landscapes therefore closely resemble allowed diversity observed in natural sequences (25).

Here, we determine Env sequence preferences independent of infection and virus propagation for interactions with three protein ligands that act as conformational probes: CD4, which induces the open Env conformation and binds monomeric gp120 with highest affinity; bNAb VRC01, which binds tightly to both monomeric gp120 and mature Env without inducing the open conformation; and bNAb PG16, which preferentially binds closed trimeric Env (1, 26–32). The mutational scans provide detailed landscapes for how sequence relates to Env conformation, in particular highlighting how electrostatic repulsion at the apical tips and underpacking at the gp120 inner-outer domain interface contribute to conformational change. We identify mutations that increase presentation of the PG16 quaternary epitope in full-length Env sequences

Downloaded from https://journals.asm.org/journal/jvi on 24 February 2022 by 65.21.193.86.

from representative tier 1B, 2, and 3 strains in clades A, B, C, and BC recombinants, while simultaneously enhancing presentation of epitopes recognized by other broadly neutralizing antibodies, and reducing CD4 binding. Finally, we demonstrate how our methodology can be applied to investigate interactions between two proteins at the membrane (Env and matrix domain [MA]) that are both expressed by the same cell. How these results relate to the design of Env immunogens that are anchored in the plasma membrane is discussed.

RESULTS

Deep mutational scanning of HIV-1 Env from the BaL isolate. Codon-optimized Env of the BaL isolate (a tier 1B virus from clade B [33]) bound soluble CD4 (domains D1 and D2), PG16, and VRC01 by flow cytometry when expressed on human Expi293F cells. Previously, deep mutational scanning of HIV-1 receptors CCR5 and CXCR4 found only qualitative agreement between replicate experiments (34), likely in part due to under sampling the diverse mutant libraries. To increase sampling of mutations in the much larger Env protein, three separate single site-saturation mutagenesis (SSM) libraries were constructed focused on the Env N terminus, center, and C terminus. Together, the SSM libraries cover 16,332 of the possible 16,520 single amino acid substitutions.

To maintain a tight link between genotype and phenotype, the Env libraries were transfected into Expi293F cells after diluting with a large excess of carrier DNA, such that typically no more than one sequence variant is expressed per cell (34). Expression was increased by addition of an artificial intron in the 5′ untranslated region, and cotransfection with carrier DNA hypothesized to promote extrachromosomal replication of the episomal Env plasmids (35).

Expi293F cells expressing the BaL Env SSM libraries were bound to soluble CD4, VRC01, or PG16 near the apparent dissociation constants and were screened by fluorescence-activated cell sorting (FACS) for highest binding signal. The enrichment or depletion of Env mutants was determined by comparing the frequencies in the naive plasmid libraries with the transcripts in the evolved populations (Fig. 1A to C). Enrichment ratios for each amino acid substitution qualitatively agreed between replicate experiments, with higher agreement for more abundant mutations that were better sampled (Fig. 1D to F). To further explore data quality, we validated by targeted mutagenesis that 20 representative mutations depleted in both replicate selections for PG16 binding did indeed have reduced binding signal (mutations are listed in Materials and Methods). However, when 43 highly enriched substitutions were individually tested, only 21 were validated to cause a slight to moderate increase in PG16 binding signal (see Materials and Methods). Identifying rare gain-of-function mutations is therefore challenging, since they can be difficult to find among the noise of many neutral or deleterious substitutions. By comparison, conservation scores (mean of the $\log_2$ enrichment ratios for all substitutions at a specific position) were closely correlated between replicate experiments and are used to define functional sites of mutational intolerance (Fig. 1G to I).

Env sequence-activity landscapes for interacting with CD4, VRC01, and PG16. The BaL Env sequence-activity landscapes are similar whether screened for CD4, VRC01, or PG16 binding (Fig. 1A to C); this is because features of the landscapes that impact protein folding and surface expression will be shared. The highest conservation is in the gp120 inner domain and in regions maintaining noncovalent association between gp41 and gp120 subunits. Polar substitutions within the hydrophobic transmembrane (TM) helix are appropriately depleted, as are extracellular premature stop codons. However, within the cytosolic tail there are regions where stop codons are tolerated or enriched, most notably between residues 731 and 759, a region that has previously been targeted with nonsense mutations for elevated Env surface expression (36–38). Interestingly, stop codons are depleted at cytosolic sites approximately corresponding to the lentivirus lytic peptide-2 (LLP-2) and LLP-3 to LLP-1 regions, even though most

Downloaded from https://journals.asm.org/journal/jvi on 24 February 2022 by 65.21.193.86.

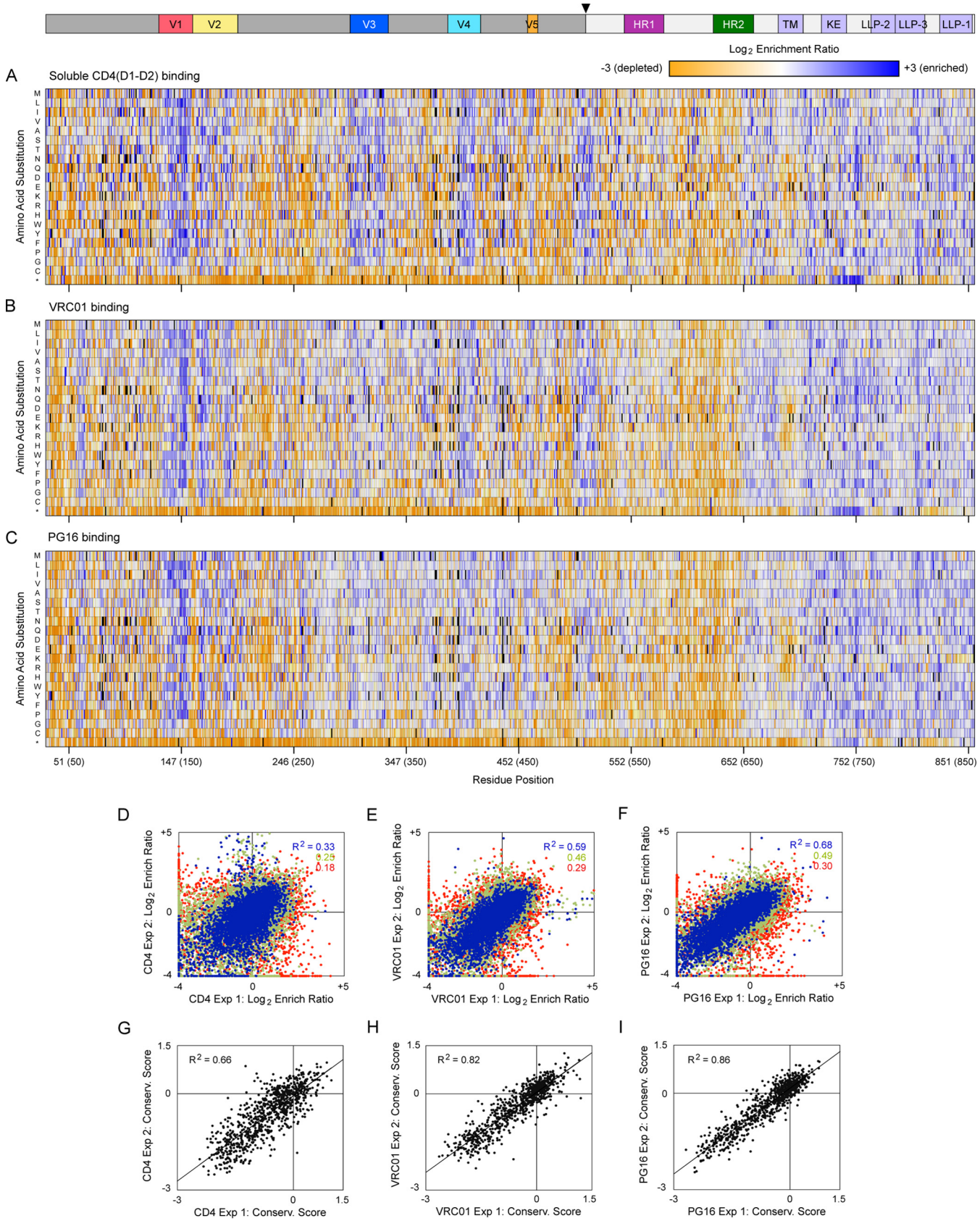

FIG 1 Mutational landscapes of BaL Env interacting with protein ligands. (A to C) Merged data from *in vitro* evolution of three SSM libraries that together fully span the mature Env_{BaL} protein. The libraries were evolved by FACS for high binding signals to 200 nM CD4(D1-D2) (A), 5 nM VRC01 (B), and 2 nM PG16 (C).

(Continued on next page)

Downloaded from https://journals.asm.org/journal/jvi on 24 February 2022 by 65.21.193.86.

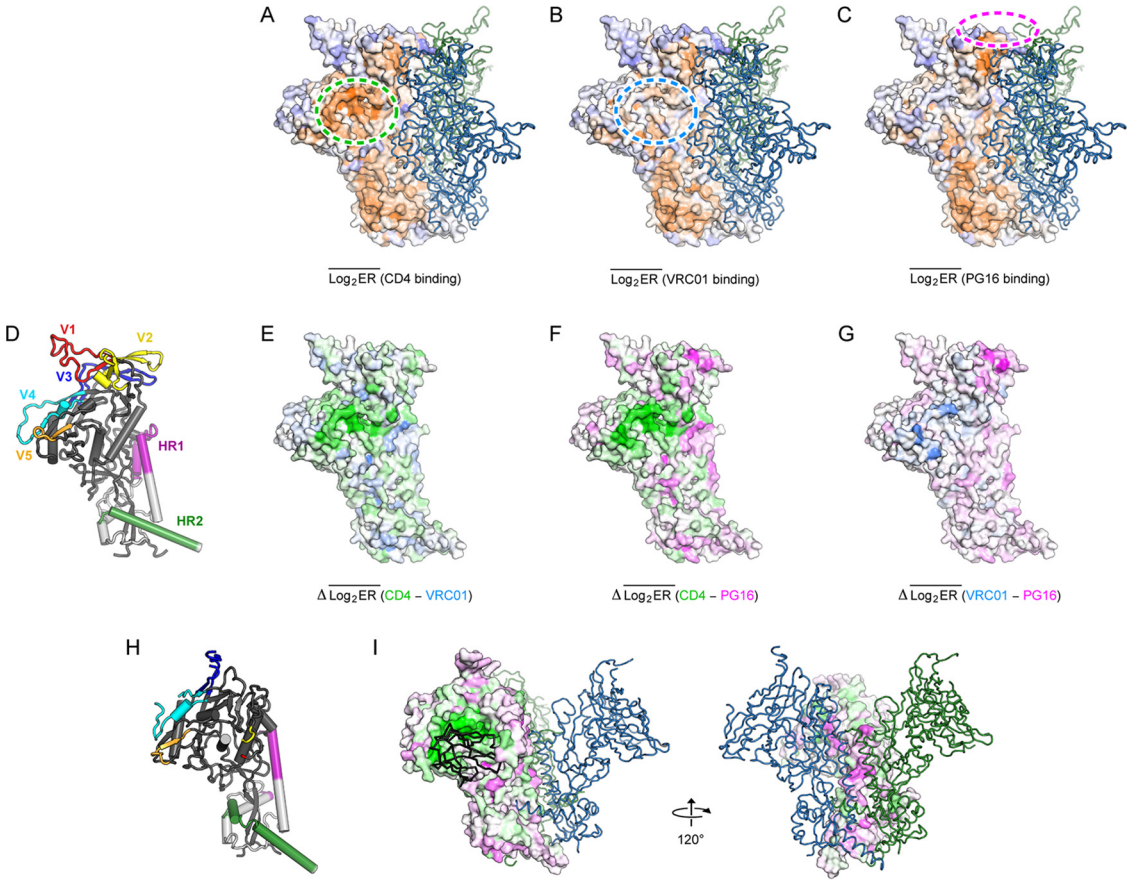

FIG 2 Mapping conserved sites for ligand binding to Env structure. (A to C) Conservation scores from selecting Env libraries for binding soluble CD4 (A), VRC01 (B), or PG16 (C) are mapped to the surface of an Env protomer, from ≤–2 (conserved, orange) to ≥+2 (under selection for change, dark blue). The second and third protomers in the trimeric spike are shown as dark green and blue ribbons. The binding sites for CD4, VRC01, and PG16 are shown with green, cyan, and magenta dashed lines, respectively. The model of BaL Env in the closed state was generated by sequence threading to PDB 5FYK, followed by loop building and side chain and backbone minimization. (D) Cartoon representation of a single protomer (gp120 is dark gray, gp41 is pale gray), oriented as in panels A to C. (E) Differences between conservation scores for binding soluble CD4 and VRC01 are plotted from –2 (more conserved for CD4 binding, green) to +2 (more conserved for VRC01 binding, cyan) on the surface of an Env protomer oriented as described above. (F) CD4-PG16 difference conservation plot colored from –2 (more conserved for CD4 binding, green) to +2 (more conserved for PG16 binding, magenta). (G) VRC01-PG16 difference conservation plot colored from –2 (more conserved for VRC01 binding, cyan) to +2 (more conserved for PG16 binding, magenta). (H) Model of Env_{BaL} in the open CD4-bound conformation (based on PDB 5VN3 [42]), showing a single protomer. (I) As in panel F, but now plotting the CD4-PG16 difference conservation scores to Env_{BaL} in the open CD4-bound conformation, oriented as in panel H. A single CD4 domain D1 is shown as a black ribbon.

amino acid substitutions are tolerated in these regions, suggesting a lack of compact folded structure.

Unique features in the respective mutational landscapes are apparent when the conservation scores are plotted on a model of trimeric BaL Env (Fig. 2A to C). To highlight regions explicitly conserved for interacting with different ligands, difference plots were mapped to the structure, in which conservation scores for interacting with one ligand are subtracted from those for interacting with a second (Fig. 2D to G). The

FIG 1 Legend (Continued)

The Env sequence is on the horizontal axis (HXB2 numbering, BaL numbering in parentheses), and single amino acid substitutions are on the vertical axis. *, Stop codon. Log_2 enrichment ratios are plotted from ≤–3 (depleted, orange) to 0 (neutral, white) to ≥+3 (enriched, blue). Mutations missing in the libraries (frequencies $< 5 \times 10^{-6}$) are black. The primary structure of gp120 (dark gray) and gp41 (light gray) is indicated above, with an arrowhead at the proteolysis site. Averages of two independent selection experiments are shown. (D to F) Correlation plots of mutation log_2 enrichment ratios from independently replicated selections for high binding signals to soluble CD4 (D), VRC01 (E), and PG16 (F). Abundant mutations (frequencies $> 2 \times 10^{-4}$ in the naive library) are blue, mutations with moderate representation (frequencies between 5×10^{-5} and 2×10^{-4}) are green, and rare mutations (frequencies between 5×10^{-6} and 5×10^{-5}) are red. (G to I) Conservation scores were calculated by averaging the log_2 enrichment ratios for all substitutions at each residue position. Conservation scores for libraries sorted for binding soluble CD4 (G), VRC01 (H), and PG16 (I) show agreement between replicate experiments.

Downloaded from https://journals.asm.org/journal/jvi on 24 February 2022 by 65.21.193.86.

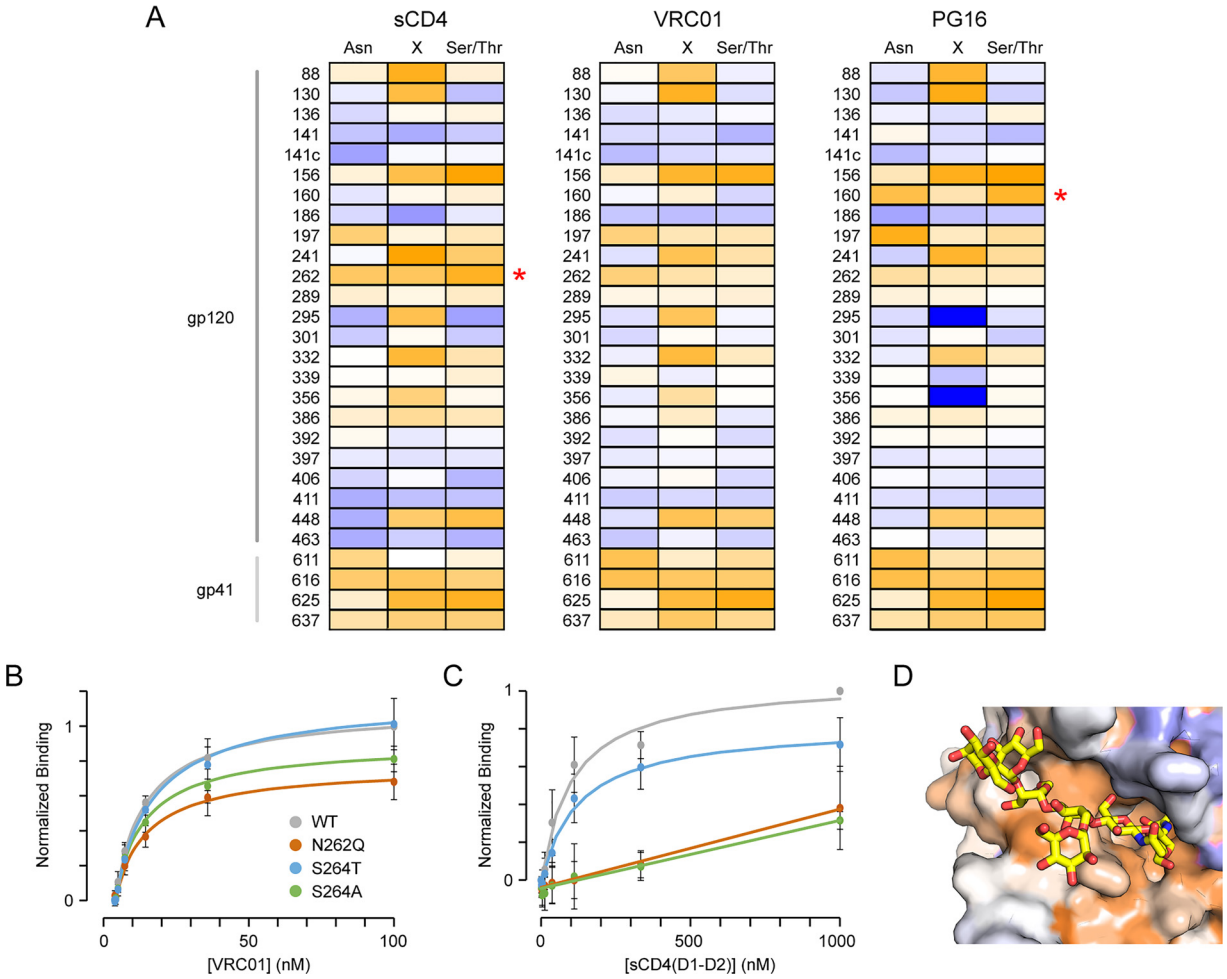

FIG 3 Conservation of N-glycosylation sites. (A) Env libraries were evolved for binding soluble CD4, VRC01, and PG16 as indicated. Conservation scores of residues within N-glycosylation motifs are plotted from −2 (conserved, orange) to 0 (variable, white) to +2 (under selection for change, blue). Site numbering is based on Asn in the motif. Red asterisks indicate glycosylation sites preferentially conserved for binding only one of the three ligands. (B) Flow cytometry analysis of VRC01 binding to Expi293F cells expressing wild-type (WT, gray), N262Q (dark orange), S264T (blue), and S264A (green) Env variants ($n = 4$, means ± the standard deviations [SD]). (C) Binding of soluble CD4 to Env variants ($n = 4$, means ± the SD). (D) The N262 glycan (yellow sticks) occupies a cleft in the cryo-electron microscopy structure of CD4-bound Env (PDB 5VN3). The protein surface is colored by conservation score for CD4 binding, from ≤−2 (conserved, orange) to ≥+2 (under selection for change, dark blue).

most notable differences are localized to the structurally characterized VRC01 and PG16 epitopes, the known CD4 binding site, and trimer interfaces. The data are in close agreement with prior structural and mutagenesis studies of the respective interactions (30, 39–42) and highlight how PG16 and especially VRC01 primarily make sequence-independent contacts that tolerate many Env amino acid substitutions.

Glycosylation sites preferentially conserved for CD4 or PG16 binding. Env is heavily glycosylated on asparagine residues at canonical NX(S/T) motifs. Of the 28 predicted Env_{BaL} N-glycosylation sites, only a small subset are moderately to highly conserved in the mutational landscapes (Fig. 3A). The four N-glycosylation sites in gp41 are similarly conserved for CD4, VRC01, and PG16 interactions, suggesting these are necessary for appropriate Env folding and surface expression. However, within gp120, glycosylation of N262 stands out as being more highly conserved for CD4 binding. N262 mutations were previously identified as reducing CD4 interactions due to diminished Env packaging into virions (43, 44). Our deep mutational scan suggests N262 site mutants also have an intrinsic CD4 binding deficit. N262Q and S264A mutants were found to have substantially reduced CD4 interactions compared to the wild type (WT) and Env S264T, which could not be explained by a large loss of protein expression

Downloaded from https://journals.asm.org/journal/jvi on 24 February 2022 by 65.21.193.86.

(Fig. 3B and C). The N262 glycan fits in a deep cleft bridging the outer and inner domains (45) that is remodeled during the closed to open conformational transition (42). Other residues lining this cleft are highly conserved for CD4 interaction (Fig. 3D).

Crystal structures of PG16 and related bNAb PG9 bound to scaffolded V1-V2 demonstrate extensive contacts to the glycan on Env-N160, with a smaller contact surface to the adjacent glycan on Env-N156 (alternatively, N173 in other HIV-1 strains) (39, 46). This is supported by mutagenesis (27). Accordingly, the N160 glycosylation motif is uniquely conserved in our mutational landscape for PG16 binding (Fig. 3A).

Env residues at the trimer interface are under selection for PG16 binding. PG16 binds the junction between two gp120 subunits at the Env apex, possibly forming bridging contacts to glycans from each subunit and explaining the antibody's preference for trimeric quaternary structure (28). When the BaL Env library is evolved for PG16 interactions, trimer interface residues are under selection and show moderate sequence conservation (Fig. 2F, G, and I), further supporting the claim that PG16 binds with highest affinity to closed trimers. We therefore hypothesized that Env may be stabilized in closed, trimeric conformations by mutations that increase PG16 binding. Extensive efforts have been invested in stabilizing closed SOSIP trimers, frequently using recognition by trimer-specific bNAbs such as PGT145 as indicators of successful engineering (47). However, PGT145-class antibodies insert a long HCDR3 loop into the Env apical cavity to make direct contacts at the apical trimer interface (48). We reasoned that by using PG16, which binds to the outer surface of trimeric Env, we might identify mutations within the apical cavity that stabilize the closed conformation, despite loss of atomic contacts to PGT145, and thereby complement previous engineering studies.

Nearly a hundred mutations in the Env sequence-activity landscape for PG16 binding had $\log_2$ enrichment ratios greater than 1.5 in both selection replicates, though we note that because most substitutions in the N-terminal SSM library were severely depleted, neutral substitutions in V1-V2 could be misleadingly enriched. We initially focused on mutations at subunit interfaces and validated 18 as causing a slight to moderate increase in PG16 binding, which are clustered at three sites (Fig. 4A; a fourth site at subunit interfaces identified from the mutational scan of $gp140_{DU422}$ will be described later). We refer to these as quaternary epitope selected (QES) mutations. The first and most prominent site is located at the trimerization interface near the apex, and includes Q114A, K117V/Y, P124D, T163D, R166E/F/L, V200E/T, R315A/Q, and R432T. Nearly all of these mutations reduce positive charge within the apical cavity. Furthermore, nearly all substitutions of Env-K117, R166, and R432 are predicted to enhance PG16 binding in the mutational landscape. This unambiguously highlights that neutralization of the electropositive apical trimer interface stabilizes a conformation with increased PG16 binding signal, and electrostatic repulsion between apical tips likely primes the subunits for conformational changes upon receptor binding. This same hypothesis was recently proposed based on the structure of BG505 SOSIP bound to bNAb PGT145 (48).

The second interfacial site of mutations for enhanced PG16 binding is a centrally located contact between Env protomers and between gp41 and gp120 subunits (Fig. 4A). F223Y in one Env protomer may add a hydrogen bond contact to R557 or N553 from a neighbor. R557Q reduces the desolvation penalty of burying a charged group at the interface, while conversely T49D or L581D can add favorable electrostatic interactions.

Mutation I595M is found at the third interfacial site. I595 of one gp41 subunit occupies a hydrophobic pocket on an adjacent gp41; the methionine substitution may better pack in this pocket (Fig. 4A).

We combined mutations to engineer BaL Env for enhanced PG16 binding (Table 1). High PG16 binding was generally achieved by combining mutations from separate sites, suggesting mutations within a single site have epistatic interactions. Two sequences, termed BaL-QES.i01 and BaL-QES.i02 ("i" for "interfaces," where most of these mutations are localized), were found to increase PG16 binding at saturation, with only

Downloaded from https://journals.asm.org/journal/jvi on 24 February 2022 by 65.21.193.86.

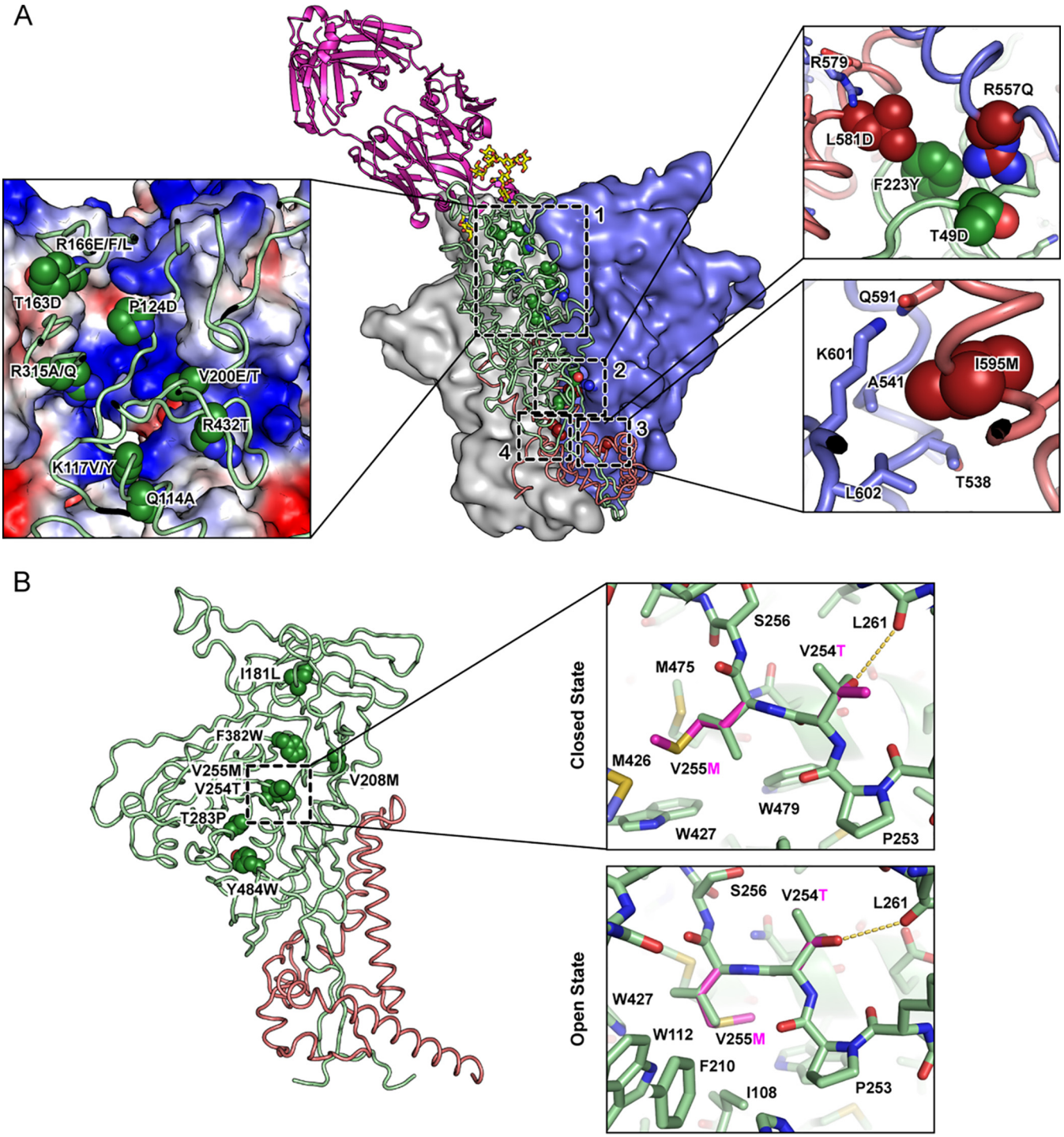

FIG 4 Neutralization of the electropositive apical cavity and increased packing at the inner-outer domain interface increase presentation of Env in a PG16-recognized conformation. From the mutational scan of $gp160_{BaL}$ and $gp140_{DU422}$, substitutions were identified and validated that enhance PG16 binding. (A) Mutations at subunit interfaces clustered to four sites, shown on a structural model of closed Env_{BaL}. PG16 is magenta, interacting glycans are yellow, two Env protomers are shown as gray and blue surfaces, and the third Env protomer is shown as green (gp120) and brick red (gp41) ribbons. In the magnified inset of site 1, the electrostatic potential on the surface of two Env protomers is plotted from positive (blue) to negative (red). Previously described mutation L544Y is found at site 4. (B) Mutations in the core generally increased hydrophobic packing along the inner-outer domain interface of gp120. In the magnified insets, V255M (magenta) fills a void in the closed conformation, whereas modeling predicts V255M has steric clashes in the open conformation, with only a single methionine rotamer being accommodated.

Downloaded from https://journals.asm.org/journal/jvi on 24 February 2022 by 65.21.193.86.

TABLE 1 Summary of mutations in first-generation Env-QES variants

Strain	Clade (tier)	Variant	Subunit interface mutations	Core mutation(s)
BaL	B (1B)	BaL-QES.i01	T49D + P124D + I595M	None
		BaL-QES.i02	T49D + P124D + L663N	None
		BaL-QES.i01.c01	T49D + P124D + I595M	I181L + V255M
Q769.d22	A (2)	Q769-QES.i03	A200E + F223Y + I595M	None
		Q769-QES.i03.V255M	A200E + F223Y + I595M	V255M
Q842.d12	A (2)	Q842-QES.i04	P124D + F223Y + R557Q + I595M	None
		QES.i04.I181L	P124D + F223Y + R557Q + I595M	I181L
25711	C (1B)	25711-QES.c02	None	I181L + V254T
DU422	C (2)	DU422-QES.c03	None	V181L + V254T + V255M

slightly tighter apparent affinities (Fig. 5A). This is consistent with expression of diverse conformations on the cell surface that do not substantially interconvert on the timescale of the experiment, and the QES mutations increase the pool of Env occupying a closed trimeric state competent for PG16 interaction. However, cells expressing these engineered variants still bound CD4 (Fig. 5B) and antibodies targeting V3 epitopes (Fig. 6A) at similar levels to wild-type Env. We reasoned that mutations predicted to positively stabilize the closed state due to improved interface complementarity are insufficient to prevent induction or sampling of the open conformation, and additional mutations are required that actively destabilize the open state by steric hindrance. Due to the form of the Lennard-Jones potential, steric clashes can have an outsized effect on the energy gap between conformational states.

A QES mutation within the core of Env can destabilize the CD4-bound state. Based on the deep mutational scan, we tested and validated three mutations within the Env core for enhanced PG16 binding (Fig. 4B). I181L is just below the surface of the apical tip where PG16 binds and perhaps stabilizes local packing. V254T and V255M are centrally positioned in the linker connecting the inner and outer domains of gp120. V254T adds a hydrogen bond to the backbone carbonyl of L261 in strand $\beta 9$ of the outer domain, while V255M increases hydrophobic packing to aromatic residues in the inner domain (Fig. 4B). The cavity occupied by V255M collapses in the open conformation with insufficient space for large hydrophobics. V255M is therefore unique among the QES mutations described thus far in that modeling predicts it also destabilizes the open state via introducing steric strain. It is notable that the Env V255M mutation was also identified in an *in vitro* replication screen for HIV-1 variants resistant to CD4 binding site inhibitors (49); resistance was also associated with reduced entry efficiency, and gp120-V255M had substantially decreased affinity for CD4 (49).

Core mutations were combined with the previous QES mutants at the trimer interface to generate BaL-QES.i01.c01 ("c" for "core"), which, when expressed on the cell surface, displays enhanced binding to PG16 and decreased binding to CD4 (Fig. 5A and B). BaL-QES.i01.c01 also has reduced exposure of V3 region epitopes (Fig. 6B), consistent with destabilization of the open conformation.

QES mutations are transferable to other Env strains and enhance binding to some bNAbs. Most of the QES mutation sites are conserved across HIV-1 strains and clades, though in some cases other strains already carry the substituted amino acid, such as a threonine, tyrosine, or glutamine at positions 200, 223, or 315, respectively. We experimentally tested whether a subset of the mutations in BaL Env that enhance PG16 binding are effective in HIV-1 strains from clades A and C (Table 1). Q769.d22 and Q842.d12 are tier 2 strains from clade A, and 25711 and DU422 are tier 1B and 2 strains from clade C, respectively (33). QES mutations at the trimer interface were effective in the clade A but not clade C sequences, while at least one core mutation could be transferred to each of the strains. As observed for BaL Env, changes in the equilibrium dissociation constant (K_D) are small, whereas PG16 binding at saturation is substantially increased (Fig. 5A), consistent with putative stabilization of the closed conformation

Downloaded from https://journals.asm.org/journal/jvi on 24 February 2022 by 65.21.193.86.

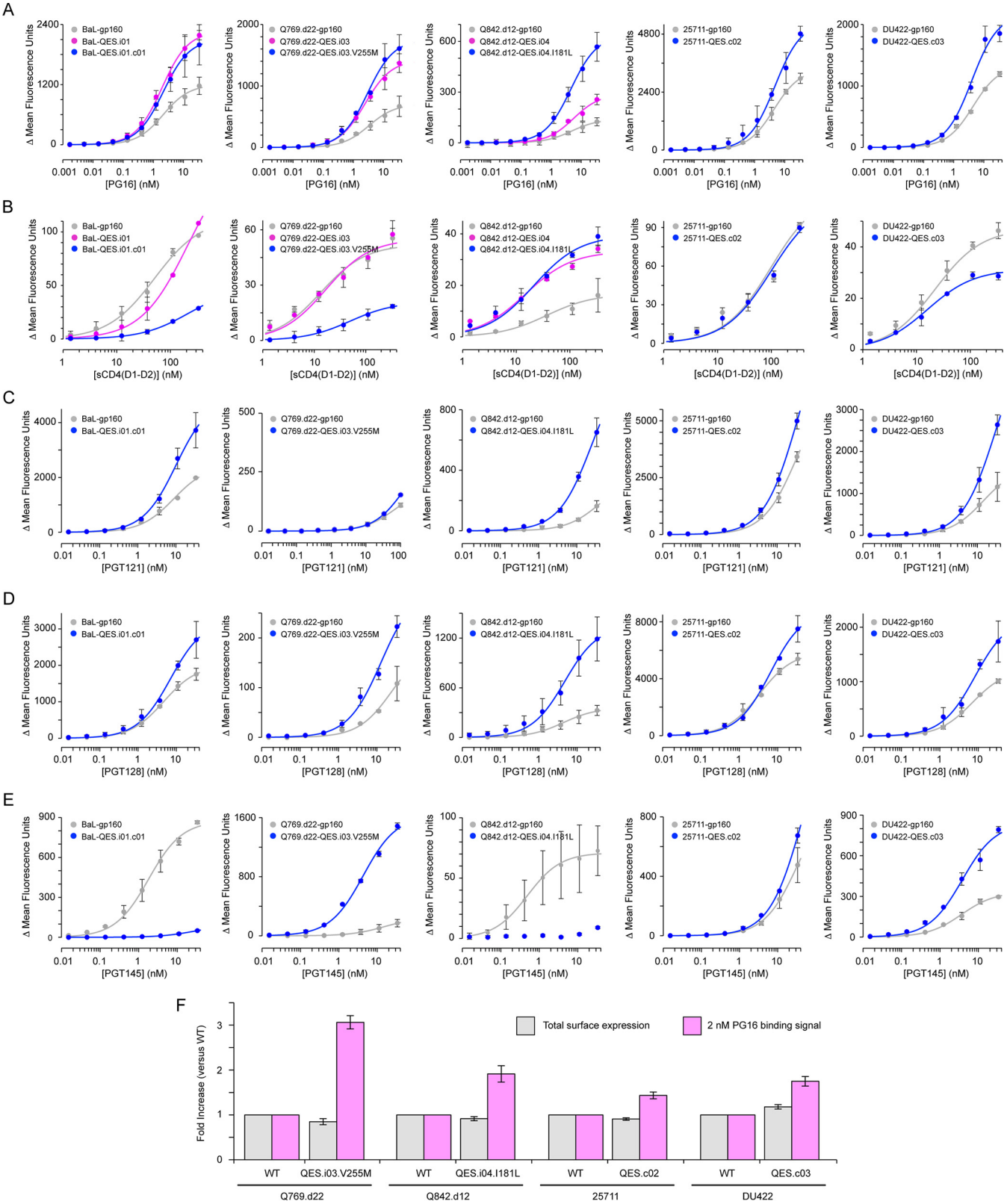

FIG 5 First generation of engineered Env proteins for enhanced presentation of the PG16-recognized conformation. (A) Expi293F cells expressing QES variants containing mutations to subunit surfaces (magenta), or additional mutations to core residues (blue), bind more PG16 than wild-type Env (gray). Env variants were tested from five HIV-1 strains (from left to right: BaL, Q769.d22, Q842.d12, 25711, and DU422). The data are means ± the SD ($n = 3$ to 4). (B) Binding of CD4(D1-D2) to cells expressing Env variants. Inclusion of the V255M core mutation in constructs BaL-QES.i01.c01, Q769.d22-QES.i03.V255M, and DU422-QES.c03 reduces CD4 binding. The data are means ($n = 2$), with error bars showing the range. (C to E) Binding of PGT121 (C), PGT128 (D), and PGT145 (E) to transfected

(Continued on next page)

Downloaded from https://journals.asm.org/journal/jvi on 24 February 2022 by 65.21.193.86.

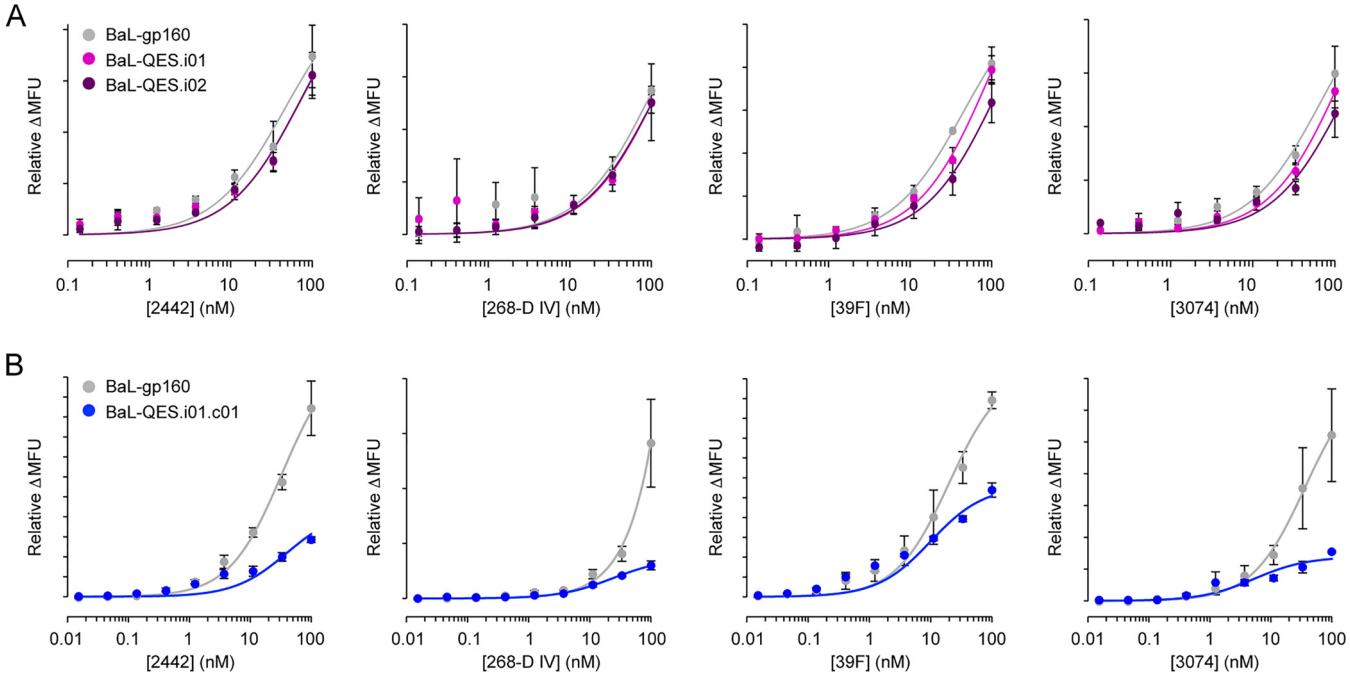

FIG 6 QES mutations at Env_{BaL} subunit interfaces are insufficient to prevent recognition by V3-targeting antibodies. (A) Expi293F cells expressing wild-type BaL (gray), BaL-QES.i01 (magenta), or BaL-QES.i02 gp160 (purple) were incubated with anti-V3 region monoclonal antibodies (from left to right) 2442, 268-D IV, 39F, and 3074. Bound antibody was detected by flow cytometry ($n = 3$, means ± the SD). (B) Binding of V3-targeting antibodies to cells expressing wild-type (gray) or QES.i01.c01 (blue; containing additional core mutations that limit CD4 interactions) BaL Env. The data are means ($n = 2$), with error bars showing the range.

increasing the fraction or total amount of folded Env on the cell surface recognized by PG16. Only variants harboring V255M had reduced CD4 binding (Fig. 5B), again emphasizing that substitutions modeled as positively stabilizing the closed state are insufficient to prevent dynamic sampling or induction of the CD4-bound open state, which instead requires explicit destabilization.

While engineering of Env was based on maximizing binding signal to a single conformation-dependent antibody, the QES variants also have increased presentation of tertiary epitopes recognized by bNAbs PGT121 and PGT128 (Fig. 5C and D), which contact the N332 glycan supersite on the outer surface of gp120 (50–53). The N332 glycan epitope is recognized by a variety of bNAb clones that originated from various germ line precursors in different individuals, implying that this structural region may form a supersite of vulnerability for immune targeting. PGT145, which makes salt bridges between acidic residues on a CDR loop and basic amino acids in the apical cavity (48), has either increased or decreased binding to the different QES constructs (Fig. 5E), reflecting antagonism between stabilization of the closed conformation (which will enhance PGT145 binding) versus amino acid changes that disrupt direct antibody contacts (specifically, decreased PGT145 binding is perfectly correlated with the inclusion of mutation P124D in the apical cavity). Since gains in PG16, PGT121, and PGT128 binding could in part be due to increases in Env surface expression, we fused c-*myc* tags to the extracellular N termini, followed by a 14-residue glycine/serine-rich linker connecting to the first residue of gp120, and measured Env surface expression independent of any folded structure. Cells expressing myc-tagged or untagged Env proteins bound PG16 similarly, with QES variants showing robust increases in PG16

FIG 5 Legend (Continued)

cells expressing wild-type or QES variant Env sequences. The data are means ($n = 2$), with error bars showing the range. (F) Wild-type and QES variants of Env were expressed with N-terminal c-*myc* tags. Total surface expression (gray; detected using fluorescent anti-myc staining) and PG16 binding (magenta; 2 nM PG16) to the same transfected cell samples were measured by flow cytometry. Mean fluorescence is normalized to cells expressing the respective wild-type Env. The data are means ± the SD ($n = 4$). Expression of BaL Env with an N-terminal c-*myc* tag was not detected and is not plotted.

Downloaded from https://journals.asm.org/journal/jvi on 24 February 2022 by 65.21.193.86.

binding (Fig. 5F). There was no apparent increase in total surface expression (Fig. 5F), consistent with a shift in the conformational ensemble expressed on the cell surface toward closed trimeric states recognized by bNAbs.

A deep mutational scan of DU422 gp140 for binding to CD4 and PG16. Ideally, we would identify a suite of mutations for applying broadly to Env from any HIV-1 strain to increase surface presentation of closed trimers that expose conserved epitopes. However, the QES mutations described thus far, based on the deep mutational scan of BaL Env, were only partially transferable to other strains. In particular, mutations that neutralize electropositive charge in the apical cavity failed to increase presentation of the PG16-recognized conformer in clade C Env sequences, despite clade C Env sharing similar electrostatic properties at the apex. To address this shortcoming, we mutationally scanned clade C DU422 Env for binding to CD4 and PG16 and identified new substitutions for an expanded set of QES mutations against which Env from any strain can be screened.

When transfected with a large excess of carrier DNA to limit the copy number of coding sequences acquired per cell, DU422 gp160 surface expression in Expi293F cells was not detected. Expression remained undetectable even when the coding sequence was downstream of an intron or when $gp160_{DU422}$ was cotransfected with carrier DNA designed to promote episomal plasmid replication. Since the cytoplasmic tail of gp160 features multiple motifs that diminish surface expression (54), we expressed only extracellular $gp140_{DU422}$ (amino acids [aa] N31 to N677) anchored to the membrane via a flexible Gly/Ser-rich linker and canonical transmembrane helix. Soluble gp140 has increased conformational heterogeneity and imperfectly mimics the ectodomains of full-length Env (11, 55, 56), and therefore we have been careful to subsequently validate interesting mutations in the full protein. DU422 gp140 was expressed on the cell surface at high levels based on flow cytometric analysis of PG16 and soluble CD4 binding.

Three SSM libraries spanning $gp140_{DU422}$ residues N31 to N279, N280 to Q577, and T578 to N677 together encoded all possible 12,820 single amino acid substitutions. As described for the mutational scan of $gp160_{BaL}$, Expi293F cells were transfected with the libraries, selected by FACS for sCD4 and PG16 binding, and mutation frequencies in RNA transcripts were compared to the naive plasmid libraries (Fig. 7A and B). Sorting experiments were independently replicated, and the $\log_2$ enrichment ratios for each mutation weakly agree; neutral mutations in the correlation plots are clustered near the origin, while deleterious mutations fall in the negative quadrant (Fig. 7C and D). Residue conservation scores are better correlated between replicates (Fig. 7E and F).

The closed state of $gp140_{DU422}$ imposes tight conservation on the apical trimerization domain. When the $gp140_{DU422}$ sequence is under selection for sCD4 binding, diversity is tolerated in variable regions V1 to V5, in residues adjacent to the furin cleavage site, within heptad repeat HR1, and downstream of heptad repeat HR2 or MPER (Fig. 7A). Strikingly, conservation extends into V1, V2, V3, and HR1 when $gp140_{DU422}$ is selected for PG16 interactions (Fig. 7B), precisely the regions that make interprotomer contacts in trimeric Env (57–62). This stringent selection of residues at the trimer interface is further illustrated when PG16-CD4 difference conservation scores are mapped to atomic models of $gp140_{DU422}$ in the closed and open states (Fig. 7G and H). Even though PG16 primarily makes sequence-independent contacts to glycans on the upper apical surface (39), DU422 gp140 residues preferentially under tight conservation for PG16 binding span almost the entire trimer interface and continue deep within the folded core of the apical trimerization domain (Fig. 7G), dramatically emphasizing that the V1, V2, and V3 regions are constrained in sequence space for adopting the trimeric PG16-recognized closed conformation. This starkly contrasts with BaL gp160, where PG16 binding is not only more tolerant of mutations in V1, V2, and V3, but many mutations in these regions can also enhance presentation of the PG16 quaternary epitope. This is likely due to both strain-specific sequence constraints (for example, the conformational equilibria of tier 2 Env proteins are shifted toward the

Downloaded from https://journals.asm.org/journal/jvi on 24 February 2022 by 65.21.193.86.

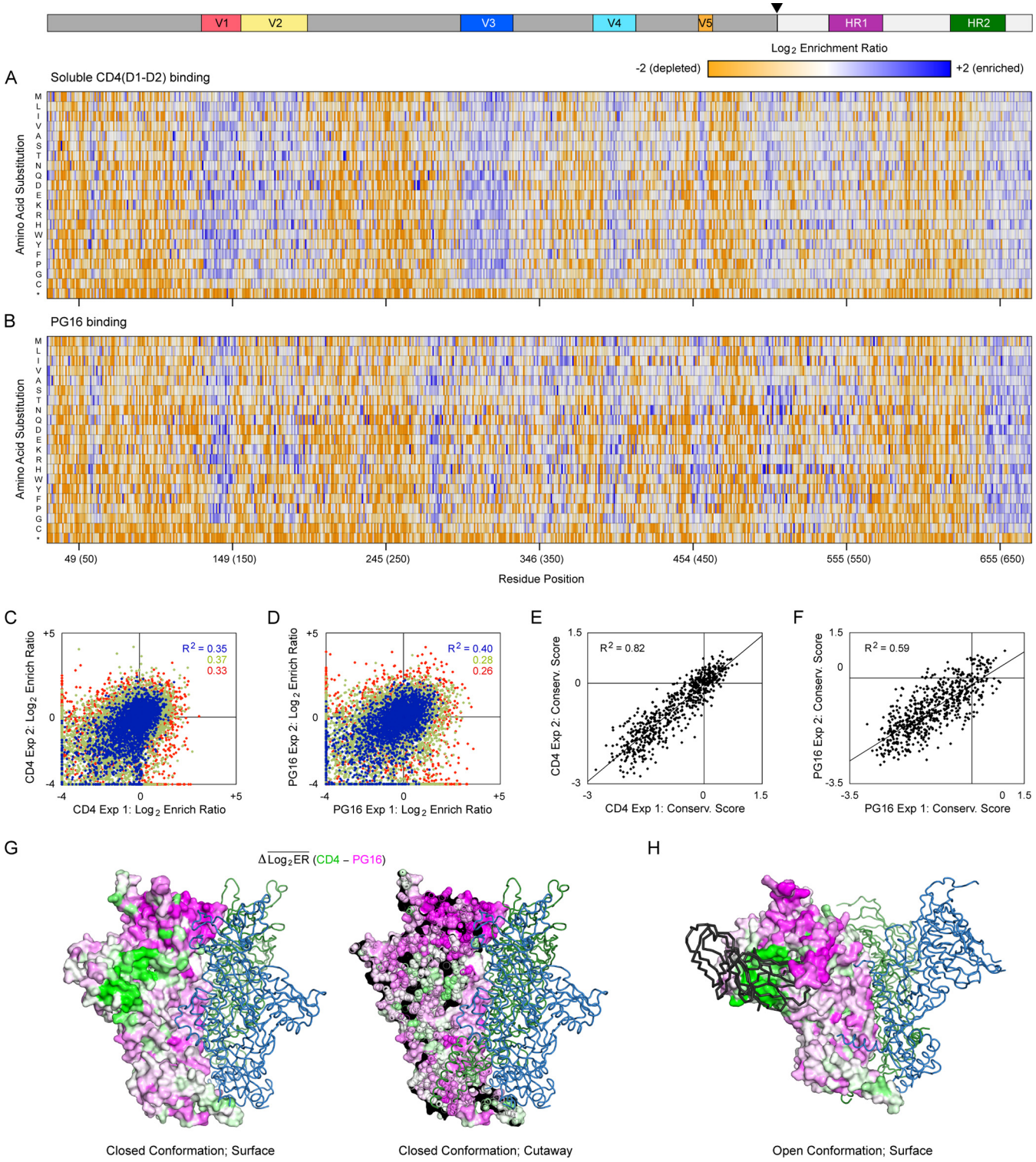

FIG 7 Residues at the Env_{DU422} trimer interface are more conserved for PG16 binding than for CD4 interactions. (A) SSM libraries of membrane-anchored $gp140_{DU422}$ were expressed in Expi293F cells and sorted for binding to sCD4. Log_2 enrichment ratios are plotted from ≤−2 (depleted, orange) to ≥+2 (enriched, dark blue). The primary structure of gp140 is on the horizontal axis, and amino acid substitutions are on the vertical axis. *, Stop codons. In the upper schematic, gp120 and gp41 are dark and pale gray, respectively; the cleavage site is indicated with an arrowhead; and notable regions are colored. Averages of two independent experiments are shown. (B) Mutational landscape of $gp140_{DU422}$ under FACS-based selection for binding to PG16. (C and D) FACS-based selections for 10 nM sCD4 (C) and 3 nM PG16 (D) binding were independently replicated. Agreement between the replicate log_2 enrichment ratios for each mutation is plotted. Abundant mutations (frequencies $> 2 \times 10^{-4}$ in the naive library) are blue, mutations with moderate representation (frequencies between 5×10^{-5} and 2×10^{-4}) are green, and rare mutations (frequencies $< 5 \times 10^{-5}$) are red. (E and F) Agreement between the residue conservation scores from replicate selections for sCD4 (E) or PG16 (F) binding. (G) An atomic model of trimeric DU422 gp140 in the closed conformation, with one protomer shown as a surface, and the other protomers shown as dark green and blue ribbons. The PG16-CD4 conservation difference scores are mapped to the protomer surface in the same

(Continued on next page)

Downloaded from https://journals.asm.org/journal/jvi on 24 February 2022 by 65.21.193.86.

closed state compared to the more open conformers that dominate tier 1B Env [63]) and also differences between gp140 versus gp160. Extracellular gp140 has an unstable structure with substantial conformational diversity, and a sizeable protein fraction likely adopts nonnative conformations (11, 14, 55, 56, 64). The trimeric closed state of gp140 may therefore be more sensitive to mutational insults than full-length gp160.

Cavity-filling mutations at the gp120 inner-outer domain interface can increase presentation of the PG16-recognized closed trimer. Based on predictions from the deep mutational scan, we screened and validated five new QES mutations in full-length DU422 gp160 that show increased PG16 binding when expressed in Expi293F cells (Fig. 4). One of the mutations, L544Y, localizes to a fourth site at the trimer interface and fills a cavity (Fig. 4A). The other four mutations (V208M, T283P, F382W, and Y484W) are at the junction between the gp120 inner and outer domains (Fig. 4B), a region where we previously identified the QES mutations V254T and V255M in BaL Env. The interface between the gp120 inner and outer domains is underpacked and undergoes substantial structural rearrangement upon CD4 ligation. As a generalization, these core mutations at the gp120 inner-outer domain interface increase hydrophobic packing. Using rational design, cavity-filling mutations have been previously described in BG505 SOSIP that stabilize closed trimers, albeit the mutations were across the entire protein rather than focused at the gp120 inner-outer domain interface (47). Our deep mutational scan was applied to an unbiased library, and it is noteworthy that the data converged on cavity-filling substitutions for enhanced presentation of the closed conformation, with two of the QES mutations we identify, L544Y and V208M, being shared with the prior study (47).

Engineered Env proteins from diverse strains for enhanced presentation of epitopes recognized by bNAbs and reduced CD4 binding. Using the expanded set of QES mutations identified from the deep mutational scanning of Env sequences from two clades, proteins were engineered from 15 different strains, spanning clades A, B, C, and BC recombinants, and tiers 1B, 2, and 3. Illustrative titration data are shown for the example of DU422 Env in Fig. 8, with data from all the engineered Env sequences listed in Table 2. In all Env sequences tested except for the clade B YU-2 strain, at least one QES mutation was effective at increasing PG16 binding when Env was expressed at the plasma membrane, and often QES mutations could be combined for further increases in PG16 binding. Neutralizing mutations in the electropositive apical cavity were only effective at increasing PG16 recognition of Env sequences from clades A and B, while core mutations were more widely applicable across strains from all the tested clades. Not only was PG16 binding to cells expressing the QES variants enhanced, but the binding of other bNAbs generally increased, too, providing further evidence that the QES mutations favor presentation of properly conformed protein. This includes increased recognition by PGT121 and PGT128 targeting the N332 glycan supersite and increased binding of PGT145 at the trimer apex except when the P124D mutation was present. Antibody 35O22, which interacts with cleaved gp41 and gp120 near the furin proteolysis site (65, 66), also showed elevated binding to cells expressing QES variants. This correlates with the observation that BG505 SOSIP.664, when purified without furin overexpression, shows increased proteolytic maturation when QES mutations are present (Fig. 9). In contrast, the binding of CD4 was reduced by cavity-filling mutations in the core.

Finally, we compared one of our QES variants, BG505-QES.i05.c06, to two published variants of BG505-SOSIP that have been tested as vaccine candidates in animal models (47). These two constructs, DS-SOSIP.4mut and DS-SOSIP.6mut, were engineered for improved thermostability, antigenic profiles, and decreased CD4 binding of soluble, purified protein. When expressed as full-length proteins, DS-SOSIP.4mut and DS-

FIG 7 Legend (Continued)

orientation as Fig. 2, with magenta indicating residues preferentially conserved for PG16 binding and green indicating residues more conserved for CD4 binding. On the right is a cross-section showing that preferential conservation for PG16 binding extends into the core of the trimerization domain. (H) DU422 gp140 modeled in the open state bound to CD4 (black ribbon; CD4 is shown bound to only a single protomer).

Downloaded from https://journals.asm.org/journal/jvi on 24 February 2022 by 65.21.193.86.

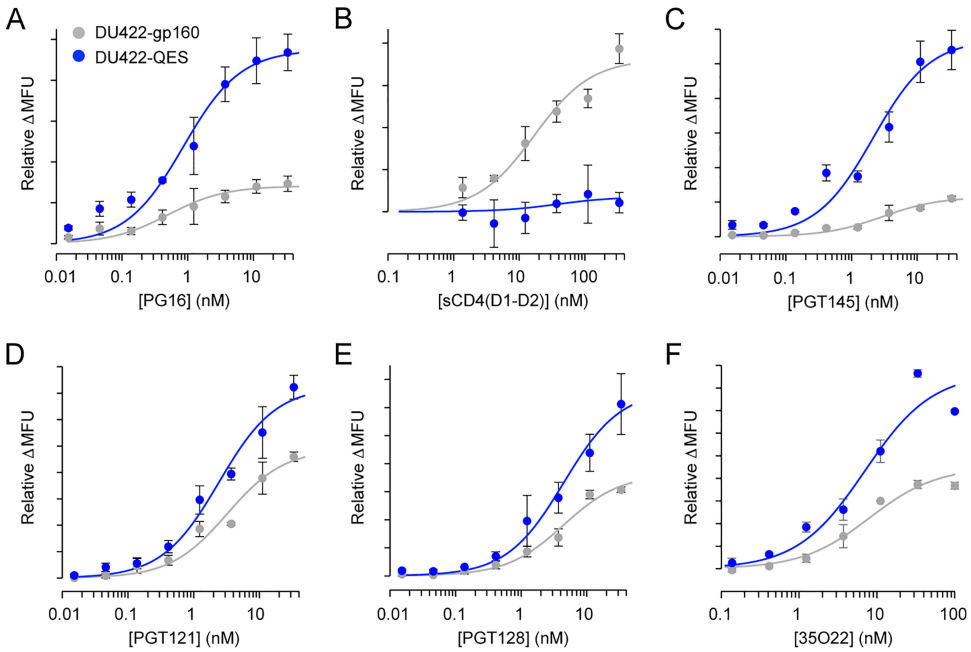

FIG 8 Antibody and CD4 binding properties of cells expressing a second-generation engineered Env from the DU422 isolate. Soluble CD4 and bNAb binding to cells transiently expressing full-length Env from the DU422 isolate was measured by flow cytometry. Wild-type Env is gray, and the engineered mutant (DU422-QES.c12 carrying seven mutations) is blue. (A) PG16; (B) sCD4 (D1-D2 domains); (C) PGT145; (D) PGT121; (E) PGT128; (F) 35O22. The data are means ($n = 2$), with error bars showing the range. Comparable binding data for engineered Envs from 15 different strains are summarized in Table 2.

SOSIP.6mut have reduced PG16 binding compared to wild-type BG505-SOSIP (Table 2), consistent with their lower yield when soluble SOSIP.664 is purified (47). This contrasts with the enhanced binding of PG16 to cells expressing BG505-QES.i05.c06, which displays only slightly higher binding to CD4 compared to the DS-SOSIP constructs (Table 2). This is not to say that BG505-QES.i05.c06 is any better or worse than DS-SOSIP but rather illustrates that by using alternative selection criteria similar yet different solutions for Env conformational engineering are reached.

A focused deep mutational scan on the Env TM and proximal cytosolic regions for possible MA association. The work described here is focused on full-length, membrane-anchored Env and might therefore be especially suitable for VLP or nucleic acid vaccines. To further increase the suitability of the engineered Env constructs, we truncated the C-terminal tails at residue 754 for elevated surface expression; this position was chosen based on high enrichment of nonsense mutations in the BaL gp160 deep mutational scans. All truncated constructs showed elevated expression (Fig. 10A).

While the details are incompletely understood, it is likely that the cytosolic tail of Env associates with the matrix domain (MA) of Gag for virus incorporation, either through direct interactions or indirectly through mediating colocalization at budding sites (67–73). To demonstrate how our deep mutational scanning methodology can be more broadly applied to address questions related to protein biophysics, we explored the possibility that sequence features in the TM and proximal cytosolic domains of Env may facilitate MA association in Expi293F cells. Using bimolecular fluorescence complementation (BiFC) (74, 75), the N-terminal half of split fluorescent Venus (VN) was fused to the end of MA, while the C-terminal half of Venus (VC) was fused to residue 753 of Env from the clade C strain 001428. This Env sequence was chosen because expression remained high after VC fusion. When 001428(753)-VC and MA-VN are in close proximity at the membrane, either due to direct or indirect association, the two halves of split Venus can fold into a competent fluorophore that is detected by flow cytometry. This experiment

Downloaded from https://journals.asm.org/journal/jvi on 24 February 2022 by 65.21.193.86.

TABLE 2 Antibody binding to cells expressing second-generation full-length Env-QES variants

Strain	Clade (tier)	Variant name	Interface mutation(s)	Core mutations	Ligand	K_D (nM)[a]		Max (QES/WT)[b]
						WT	QES	
Q769.d22	A (2)	Q769-QES.i03.c04	A200E, F223Y, I595M	V255M, F382W	sCD4	2	30	0.3
					PG16	1	0.6	3.2
					35O22	0.8	0.6	4.3
					PGT145	10	0.2	4.0
Q842.d12	A (2)	Q842-QES.i04.c05	P124D, F223Y, R557Q, I595M	I181L, V208M, T283P, F382W	sCD4	50	40	0.3
					PG16	0.2	0.1	21.0
					35O22	4	2	15.0
					PGT121	3	2	2.8
					PGT128	5	3	7.7
					PGT145	2		Only WT binds
BG505 (SOSIP)	A (2)	BG505-QES.i05.c06	A200E, F223Y, L544Y, I595M	V181L, V255M, Y484W	sCD4	9	40	0.5
					PG16	0.7	0.5	1.3
					35O22	1	0.5	2.7
					PGT121	20	16	1.3
					PGT128	7	6	1.8
					PGT145	4	6	1.1
					F105	20		Only WT binds
BG505 (SOSIP)	A (2)	BG505 DS-SOSIP.4mut		L154M, I201C, N300M, N302M, T320L, A433C	sCD4	9	70	0.4
					PG16	0.7	1	0.7
BG505 (SOSIP)	A (2)	BG505 DS-SOSIP.6mut		L154M, Y177W, I201C, N300M, N302M, T320L, I420M, A433C	sCD4	9	100	0.3
					PG16	0.7	0.9	0.5
191084 B7-19	A (2)	191084-QES.i06.c07	P124D, L544Y, R557Q	V208M, V255M, F382W	sCD4	4	50	0.2
					PG16	1	2	1.8
					35O22	1	2	3.7
					PGT121	30	20	1.4
					PGT128	7	5	1.9
					PGT145	4		Only WT binds
BaL	B (1B)	BaL-QES.i01.c08	T49D, P124D, I595M	I181L, V255M, V283P	sCD4	30		Only WT binds
					PG16	1	1	1.8
					35O22	4	4	2.0
					PGT121	4	2	1.5
					PGT128	1	2	1.8
					PGT145	0.5		Only WT binds
					447-52D	11	10	0.6
					F105	ND	ND	0.5
H031	B (2)	H031-QES.i07.c09	S49D, F223Y	V181L, V254T, V255M, F382W	sCD4	3	2	0.8
					PG16	1	2	2.6
					35O22	0.6	1	4.8
					PGT121	2	3	1.9
					PGT128	1	2	1.6
					PGT145	3	2	3.8
					447-52D	0.4	0.4	1.2
B41	B (2)	B41-V200E	V200E	None	sCD4	40	20	0.9
					PG16	20	10	1.3
					35O22	30	50	1.4
					PGT121	20	30	1.4
					PGT128	10	10	1.4
					PGT145	40	6	1.7

(Continued on next page)

Downloaded from https://journals.asm.org/journal/jvi on 24 February 2022 by 65.21.193.86.

TABLE 2 (Continued)

Strain	Clade (tier)	Variant name	Interface mutation(s)	Core mutations	Ligand	K_D (nM)[a] WT	QES	Max (QES/WT)[b]
AD8	B	AD8-QES.i08.c04	P124D, I595M, L663N	V255M, F382W	sCD4	100	70	0.4
					PG16	0.8	0.7	1.0
					35O22	3	4	1.6
					PGT121	8	3	1.0
					PGT128	1	2	1.4
					PGT145	3	10	0.5
					17b	0.4		Only WT binds
25711	C (1B)	25711-QES.c11	None	I181L, V208M, V254T, F382W	sCD4	8	3	0.5
					PG16	0.4	0.3	1.9
					35O22	0.2	0.2	2.0
					PGT121	20	20	1.5
					PGT128	3	3	1.3
					PGT145	20	50	3.0
ZM197M	C (1B)	ZM197M-QES.c10	None	V208M, V254T, V255M	sCD4	30	300	0.4
					PG16	10	10	1.2
					35O22	2	1	1.5
					PGT121	30	20	1.1
					PGT145	20	10	0.9
DU422	C (2)	DU422-QES.c12	None	V181L, V208M, V254T, V255M, T283P, F382W, Y484W	sCD4	20		Only WT binds
					PG16	0.5	0.9	3.4
					35O22	6	6	2.0
					PGT121	3	2	1.5
					PGT128	4	4	1.8
					PGT145	3	2	5.0
001428-2	C (2)	001428-QES.c10.L544Y	L544Y	V208M, V254T, V255M	sCD4	40	50	0.2
					PG16	0.3	0.8	1.3
					35O22	6	3	2.4
					PGT121	30	30	1.7
					PGT128	20	20	1.7
					PGT145	0.7	0.7	1.9
SHIV327C-Hu A10	C	HuA10-QES.i09.c07	L544Y, I595M	V208M, V255M, F382W	sCD4	5	5	0.2
					PG16	0.5	0.2	7.0
					35O22	0.2	0.2	5.0
					PGT121	4	0.9	1.6
					PGT128	0.1	0.6	1.4
					PGT145		9	Only QES binds
CH111	BC (2)	CH111-QES.c13.L544Y	L544Y	V208M, V255M, T283P	sCD4	100	400	0.5
					PG16	0.9	0.6	3.9
					35O22	0.7	0.6	2.0
					PGT121	2	4	1.3
					PGT128	5	9	1.3
					PGT145	20	9	4.8
CH115	BC (3)	CH115-QES.c14	None	V208M, V254T, V255M, I283P	sCD4	3	10	0.1
					PG16	1	1	1.2
					35O22	0.2	0.2	1.8
					PGT121	3	3	1.4
					PGT128	1	0.8	0.9
					PGT145	4	3	1.2
					17b	0.4		Only WT binds

[a]ND, not determined due to weak signals.
[b]Binding parameters (K_D and maximum binding at saturation) were calculated from curves fitted to the means from two replicates.

Downloaded from https://journals.asm.org/journal/jvi on 24 February 2022 by 65.21.193.86.

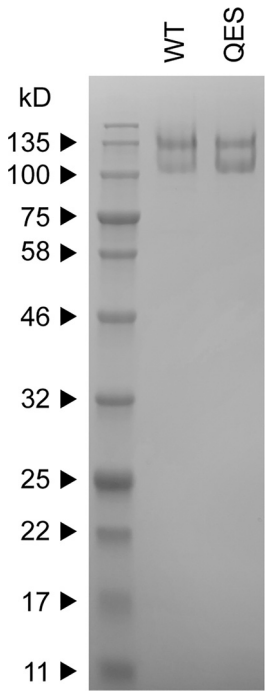

FIG 9 A QES variant of soluble BG505 SOSIP.664 has improved proteolytic maturation. Coomassie blue-stained sodium dodecyl sulfate gel of purified His_8-tagged BG505 SOSIP.664. WT, wild type. QES, first-generation QES variant containing mutations V181L, A200E, F223Y, V255M, and I595M. Based on quantification of band intensities, proteolytic processing increased from 35% of WT to 50% of the QES variant.

has a number of important limitations. First, the effects of C-terminal truncations on Env incorporation into the virus vary between cell lines, implicating possible host specific factors mediating Env/MA association (73, 76), and data from Expi293F cells may not be generalizable. Second, while MA is anticipated to be myristoylated and trimerize on membranes in the experimental system, higher-order lattice organization dependent on the capsid domain of Gag may be necessary to observe weak Env interactions through avidity (77). Finally, functional motifs may exclusively reside in the distal cytosolic tail that was deleted in this study, which was necessary to increase the expression of VC-fused Env for reliable FACS-based sorting.

An SSM library was constructed of 001428(753)-VC covering all single amino acid substitutions across residues N677 to L753, and the library was screened by FACS in an Expi293F line stably expressing MA-VN. PG16-positive cells were gated, and within this gate cell populations with high and low BiFC signals were collected (Fig. 10B) and deep sequenced. Mutations that enhance Env/MA association would be preferentially enriched in the high BiFC population (Fig. 10C), mutations that disrupt possible Env/MA interactions or colocalization would be exclusively enriched in the low BiFC population (Fig. 10D), and mutations that simply increase Env expression would be enriched in both populations. Data quality was excellent, with high reproducibility between independent replicates (Fig. 10E and F). As expected, all premature stop codons are depleted for high BiFC signal, as these remove the VC fusion. The enrichment pattern for nonsense mutations is more complex in the low BiFC population; premature stop codons prior to and within the TM helix are depleted, as these cause a loss of Env surface expression, yet premature stop codons in the cytoplasmic tail are enriched as Env surface expression is maintained but the VC fusion is lost. Polar substitutions in the TM helix tend to be depleted in both populations, indicating that they negatively impact Env surface expression, with the sole exception of R696, which tolerates all substitutions other than aspartic acid. The mutational landscape within the proximal cytoplasmic tail is featureless, and we conclude that there are no mutations in this

Downloaded from https://journals.asm.org/journal/jvi on 24 February 2022 by 65.21.193.86.

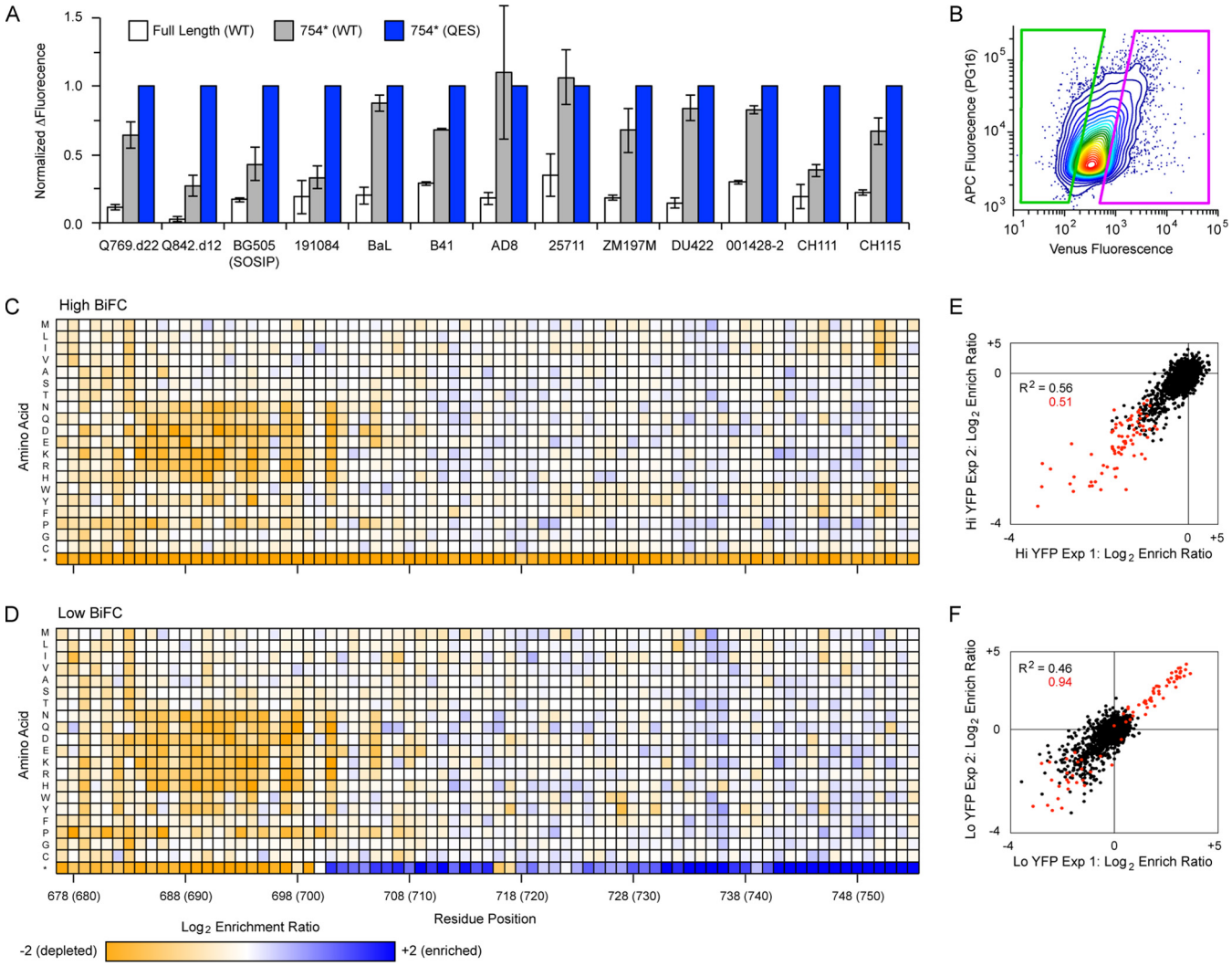

FIG 10 Mutational landscape of Env TM and proximal cytosolic regions for associating with MA. (A) Wild-type Env (WT, gray) and QES variants of Env (blue) with premature stop codons at position 754 had enhanced expression compared to full-length WT Env (white). Transfected cells were stained with a high PG16 concentration (20 nM). The data are means ($n = 2$), with error bars showing the range. (B) Cells coexpressing 001428(753)-VC and MA-VN were gated for scatter properties, viability, low autofluorescence, and PG16 binding as described in Materials and Methods. The final collection gates are shown here. Cells were sorted for high BiFC (magenta, 15% of PG16-positive population) or low BiFC (green, 15% of PG16-positive population). (C) Mutational landscape of 001428 Env colocalizing with MA based on high BiFC. Log_2 enrichment ratios are plotted from ≤−2 (depleted, orange) to ≥+2 (enriched, dark blue). Residue positions (HXB2 reference numbering, 001428 numbers in parentheses) are on the horizontal axis, and amino acid substitutions are on the vertical axis. Average of two independent replicates. (D) Mutational landscape of 001428 Env selected for low BiFC with MA. (E and F) Correlation plots for replicate experiments where cells expressing 001428 Env variants were sorted for high (E) or low (F) BiFC with MA. Nonsynonymous mutations are black; nonsense mutations are red.

region that have a critical role for Env/MA associations, though the experiment's limitations described above must also be considered.

This simple experiment effectively demonstrates how deep mutational scans that are independent of virus passaging can address important biophysical questions. Surface glycoproteins of influenza and HIV-1 have been exhaustively investigated in the past decade by deep mutational scanning, yet in nearly all cases these studies have tracked replicative viruses being passaged in culture. By using FACS as the selection pressure and decoupling the mutational scans from virus replication, we have been able to address how Env sequence relates to very specific protein activities.

DISCUSSION

Alignments of protein sequences observed in nature are very effective at revealing conserved residues in primary structure for correct folding and function. However, a natural sequence like HIV-1 Env is shaped by multiple activities; Env must fold, traffic to

Downloaded from https://journals.asm.org/journal/jvi on 24 February 2022 by 65.21.193.86.

the cell surface, be incorporated into a budding virion, bind target receptors, mediate membrane fusion, and escape antibody neutralization. Here, *in vitro* selection was instead focused on the specific activities of folding to a trimeric closed conformation and binding to the CD4 receptor. The sequence-activity landscapes provide insight into Env mutational tolerance for acquiring closed and CD4-bound conformations, information which is not at all obvious from a multiple sequence alignment. This information provided mechanistic insights and was leveraged for engineering full-length Env for enhanced presentation of vulnerable epitopes when expressed on the cell surface. By shifting the expressed conformational ensemble toward closed trimers recognized by broadly neutralizing antibodies, QES variants may prove useful for vaccines that incorporate Env in ways that cannot be easily purified in the desired conformation (e.g., VLP or nucleic acid vaccines). More importantly, this body of work highlights a mutational scanning methodology that does not require virus passaging and can be broadly applied to any complex protein expressed in human cells.

MATERIALS AND METHODS

Tissue culture. All experiments were in the CXCR4-knockout Expi293F cell line (34); these cells do not express CD4, CCR5, or CXCR4 receptors. Cells were cultured in Expi293 Expression Medium (Life Technologies) in 8% CO_2 at 37°C and 125 rpm.

Expression plasmids. Synthetic, human codon-optimized Env sequences were synthesized as gBlocks (Integrated DNA Technologies) from HIV-1 isolates Q769.d22 (GenBank accession no. AAM66234.1), Q842.d12 (AAM66242.1), BG505 (ABA61516.1; carrying the SOSIP, T332N, and 6xArg proteolysis site mutations), 191084 B7-19 (ADI62025.1), BaL (AAA44191.1), H031 (EF210728), B41 (AEO83374.1), AD8 (AAB64170.1), 25711 (ABL67448.1), ZM197M (ABD49673.1), DU422 (ABD83641.1), 001428-2 (ABL67442.1), SHIV327C-Hu A10 (AIZ78012.1), CH111 (EF117258), and CH115 (EF117263). The genes encoded mature polypeptides fused to an N-terminal CD5 leader (sequence MPMGSLQPLATLYL LGMLVASVLA), and were cloned into the NheI-XhoI sites of pCEP4. Mutations were made by overlap extension PCR.

When transfecting cells under conditions that yielded a single coding variant per cell, a pCEP4 derivative vector (pCEP4-intron) containing a strong 5′ chimeric intron was used for enhanced expression. This was created by cloning the intron from plasmid pRL-SV40 (Promega) into the KpnI-NheI sites of pCEP4.

Plasmid library construction. Single site-saturation mutagenesis (SSM) libraries were generated by overlap extension PCR (78). For the $gp160_{BaL}$ library, three separate SSM libraries were constructed focused on the Env_{BaL} N terminus (aa 31 to 265; library A), center (aa 266 to 529; library B), and C terminus (aa 530 to 856; library C). The PCR products were cloned by restriction enzyme digestion and ligation into the NheI-BglII (library A), BamHI-NotI (library B), and PstI-XhoI (library C) sites of BaLgp160 inserted into the NheI-XhoI sites of pcDNA3.1(+) (Invitrogen), with the vector PstI and BglII sites removed by QuikChange (Agilent) mutagenesis. Ligations were transformed into NEB 5-α or 10-β electrocompetent *Escherichia coli* (New England Biolabs), and plasmid DNA for each library was prepared using GeneJET Maxiprep kit (Thermo Scientific). Following library construction in the pcDNA3.1(+) vector, the full-length diversified BaLgp160 library inserts was subcloned into the NheI-XhoI sites of pCEP4-intron. At all cloning steps, the number of transformants was at least an order of magnitude greater than the possible library diversity. Combined, the three BaL gp160 SSM libraries covered 16,332 of 16,520 possible single amino acid mutations, based on a minimum frequency of 5.7×10^{-6} (corresponding to approximately 10 reads) in the deep sequenced plasmid libraries.

For the $gp140_{DU422}$ library, the gp140 ectodomain (aa N31 to N677, HXB2 reference numbering) was fused using PCR-based assembly to a C-terminal Gly/Ser-rich linker, His_6 tag, and the transmembrane helix of HLA class I α chain for surface display. The synthetic gene was cloned into the NheI-XhoI sites of pCEP4. Three separate SSM libraries were constructed focused on the N terminus (aa 31 to 279; NT library), center (aa 280 to 577; central library), and C terminus (aa 578 to 677; CT library). Mutagenized PCR segments were ligated into the NheI-Pfl23II (NT library), SbfI-HindIII (central library), or Pfl23II-XhoI (CT library) sites of pCEP4-$gp140_{DU422}$. Ligations were electroporated and plasmid DNA purified as described above. All possible 12,820 single amino acid substitutions were present in the three SSM libraries.

To investigate Env association with MA, 001428 Env with a CD5 leader peptide was genetically fused at residue L753 to the C-terminal half of split Venus (VC: aa D155 to K238) via a GGSG linker using PCR-based assembly. A 001428(753)-VC SSM library was generated by overlap extension PCR (78) and covered residues N677-L753. The library was cloned into the NheI-XhoI sites of pCEP4-intron and prepared as described above. All possible 1,540 single amino acid mutations were present.

Library transfections. DNA libraries were transfected into CXCR4-knockout Expi293F cells. For transfecting the 001428(753)-VC library, the cells also stably expressed a MA-VN fusion. The MA domain of Gag (a.a.1 to 125) from plasmid pGag-EGFP (catalog no. 11468 from the NIH AIDS Reagent Program, Division of AIDS, NIAID) (68) was fused to the N-terminal half (VN: aa V1 to A154) of split Venus (mutant I152L), a yellow fluorescent protein variant with improved signal-to-noise for the detection of protein interactions by BiFC (74). The fusion construct was cloned back in to pGag-EGFP using KpnI-NotI, and the

Downloaded from https://journals.asm.org/journal/jvi on 24 February 2022 by 65.21.193.86.

plasmid was linearized with AflIII and transfected into CXCR4-knockout Expi293F cells. Stable transfectants were selected with 100 μg/ml G418, and positive cells were enriched by FACS after transient transfection with pcDNA3.1(+) encoding VC.

The libraries were transfected such that on average no more than one coding sequence was acquired per cell (34). Cultures at a density of 2×10^6 cells/ml were transfected using Expifectamine with 1 ng/ml library DNA and 1.5 μg/ml pCEP4-ΔCMV (35) as carrier DNA. At 2 h posttransfection, the medium was replaced.

Sorting cell libraries for binding to sCD4, VRC01, and PG16. Recombinant sCD4-183 (provided by Progenics), VRC01 (32), and PG16 (27) were obtained from the NIH AIDS Reagent Program, Division of AIDS, NIAID (catalog numbers 7356, 12033, and 12150).

For CD4 binding, cells were harvested 24 to 26 h following transfection with library DNA, washed with ice-cold phosphate-buffered saline supplemented with 0.2% bovine serum albumin (PBS-BSA), and incubated on ice for 40 min with 200 nM ($gp160_{BaL}$ libraries) or 10 nM ($gp140_{DU422}$ libraries) sCD4-183. Cells were washed twice, incubated on ice for 30 min with fluorescein isothiocyanate (FITC)-conjugated anti-CD4 (clone M-T441 [LifeSpan BioSciences], 1/200 dilution), washed twice, and resuspended in PBS-BSA.

For antibody binding, the cells were washed with cold PBS-BSA at 24 to 26 h posttransfection and incubated on ice for 40 min with 5 nM VRC01 ($gp160_{BaL}$ libraries), 2 nM PG16 ($gp160_{BaL}$ libraries), or 3 nM PG16 ($gp140_{DU422}$ libraries). Cells were washed twice, incubated for 30 min with allophycocyanin (APC)-conjugated anti-human IgG Fc antibody (BioLegend, clone HP6017, 1/300 dilution), washed twice more, and resuspended in PBS-BSA.

Labeled cells were sorted on a BD FACSAria II at the Roy J. Carver Biotechnology Center. Single cells were gated based on FSC/SSC, and dead cells that were positive for propidium iodide (added to a final concentration of 1 μg/ml) were excluded. Autofluorescent cells in the APC channel (after staining with FITC-conjugated anti-CD4) or FITC channel (after staining with APC-conjugated anti-IgG Fc) were also excluded. Cells were collected with the highest fluorescent signals (the top 0.3 to 1.0% depending on the library and ligand, chosen so as to collect cells with similar binding signals across the respective libraries). Sort conditions are described in greater detail in the sequence depositions with NCBI's Gene Expression Omnibus (79). Sorted cell pellets were frozen at −80°C. To maintain cell viability and mRNA quality during the experiment, samples were sorted for a maximum of 4 h into tubes that had been coated overnight with fetal bovine serum (FBS). To collect greater numbers of cells than one 4-h sort provided, libraries were prepared again and frozen cell pellets from multiple days' experiments were pooled during RNA extraction. Each replicate typically required 8 h of sorting per library.

BiFC-based library sorting. Cells stably expressing MA-VN were transfected with the 001428(753)-VC plasmid library and stained 24 h posttransfection with 2 nM PG16 and APC-anti-IgG Fc as described above. During sorting, single cells were gated by FSC/SSC properties, and propidium iodide-positive dead cells and Pacific Blue-positive autofluorescent cells were excluded. APC-positive cells were gated, and the upper and lower 15% for Venus fluorescence (Fig. 10B) were collected into tubes that had been coated overnight with FBS.

Deep sequencing. Total RNA was extracted from sorted cells using a GeneJET RNA purification kit (Thermo Scientific), and first-strand cDNA was synthesized with high-fidelity AccuScript reverse transcriptase (Agilent Technologies) primed with oligonucleotides that annealed downstream of the diversified regions. To generate fragments for deep sequencing, the cDNA was PCR amplified in two rounds. In the first round, primer overhangs added complementary sequences to the Illumina sequencing primers. In the second round, primer overhangs added barcodes and adaptor sequences for annealing to the Illumina flow cell. Thermocycling was kept to a minimum to reduce the introduction of PCR biases and errors. Primer sequences are provided in the GEO depositions. Each of the $gp160_{BaL}$ libraries was amplified as three overlapping fragments to achieve full sequencing coverage. For $gp140_{DU422}$, the NT and central libraries were amplified as two overlapping fragments, while the CT library was amplified as a single fragment. The 001428(753)-VC library was amplified as a single fragment focused on the diversified region. DNA was sequenced at the UIUC Roy J. Carver Biotechnology Center on an Illumina MiSeq v3 (2×300nt kit) or HiSeq 2500 (2×250nt kit), and data were analyzed with Enrich (80). Log_2 enrichment ratios of mutants were normalized by subtracting the enrichment of the wild-type sequence.

Flow cytometric analysis of Env mutants binding to antibodies and sCD4. Expi293F CXCR4-knockout cells were transfected with Expifectamine (Life Technologies) using 500 ng of plasmid DNA per ml of cells at a density of 2×10^6/ml, unless stated otherwise. Transfection Enhancers (Life Technologies) were added after 18 h, and cells were analyzed ~40 h posttransfection. Cells were washed with PBS-BSA and incubated on ice for 40 min with the indicated antibodies or sCD4. Cells were washed twice, incubated for 30 min with secondary antibody (1/200 FITC-anti-CD4 clone M-T441 [LifeSpan BioSciences] or 1/300 APC-anti-IgG clone HP6017 [BioLegend]), washed twice, and analyzed on a BD LSR II flow cytometer. For titrating different antibodies or sCD4, a 1:3 serial dilution of the ligand was prepared in a 96-well round-bottom plate, and plates were incubated with the antibody at 4°C on a rocker. 39F (81, 82) was provided by the NIH AIDS Reagent Program from James E. Robinson. 268-D IV (83), 2442 (84), and 3074 (85, 86) were provided by Susan Zolla-Pazner through the NIH AIDS Reagent Program. PGT121 (87), PGT128 (87), and PGT145 (87) were provided by IAVI through the NIH AIDS Reagent Program. 35O22 (66) was provided by the NIH AIDS Reagent Program from Jinghe Huang and Mark Connors.

Assessment of data quality by targeted mutagenesis. A total of 20 representative mutations were chosen that were depleted following FACS-based selection for PG16 binding in both replicate experiments. All 20 mutants were found to have reduced PG16 (2 nM) binding signal by flow cytometry when

Downloaded from https://journals.asm.org/journal/jvi on 24 February 2022 by 65.21.193.86.

transfected in to Expi293F cells. The mutations were V36R, F93G, D133W, F159V, Y191I, S199C, I201M, V208G, F223L, T248E, I251S, T319K, C331I, W338A, I491S, Q540V, W614A, K617Q, E634A, and I686R.

A total of 43 mutations biased toward subunit interfaces and the furin cleavage site were tested by targeted mutagenesis for increased PG16 (0.5 and 2 nM) binding when expressed by Expi293F cells. All the mutations were enriched in the replicate selections for PG16 binding. Of these mutations, 21 were validated as increasing PG16 binding signals by small to moderate degrees: T49D, Q114A, K117V, K117Y, P124D, T163D, R166E, R166F, R166L, V200E, V200T, F223Y, R315A, R315Q, R432T, G514P, G516Q, R557Q, L581D, I595M, and L663N. The 22 mutations that did not increase PG16 binding were L34Y, W35Y, T51Q, Y61K, Y61Q, E106S, I161L, N164P, I165H, I165L, I165Q, T244I, V430E, K500Q, A501E, E509Q, H564A, L568Y, Q658F, E662Q, K665N, and S700Q.

Structural modeling. Homology modeling of BaL Env was based on structures of sequences from other HIV-1 strains. VRC01-bound $gp140_{BaL}$ in the closed conformation was modeled by threading the BaL strain sequence onto PDB 5FYK (88) with glycans removed and rebuilding missing loops and minimizing side chain conformations in FoldIt (89). CD4-bound $gp120_{BaL}$ was generated by threading the BaL sequence onto PDB 1GC1 (40) and minimizing side chain and backbone conformations with FoldIt. For modeling open-state $gp140_{BaL}$ bound to CD4, the sequence of BaL Env was threaded onto PDB 5VN3 (42), which was then minimized with C3 symmetry using ROSETTA (90). The model of the PG16-bound apical epitope was generated by threading the BaL sequence onto PDB 4DQO (39). Coordinates for the glycan on N160 were kept, and a single *N*-acetyl-D-glucosamine sugar was added to N156. The structure in Fig. 4 was generated by superimposing the model of the PG16-bound epitope to the model of closed Env. Homology modeling of DU422 Env was based on PDBs 5FYK and 5VN3 as described above. Images were rendered with the PyMOL Molecular Graphics System (Schrödinger, LLC).

Total cell surface expression and PG16 binding of c-*myc* tagged Env. To test for changes in total cell surface expression, the native signal peptide of Env was replaced with the influenza hemagglutinin signal peptide (MKTIIALSYIFCLVFA), followed by a c-*myc* epitope tag and 14-residue flexible linker (GSPGGASSGSGSGG) prior to the first residue of gp120. Expi293F CXCR4-knockout cells were transfected using Expifectamine with 500 ng of plasmid DNA encoding myc-tagged Env, and transfection enhancers were added 20 h posttransfection. Cells were tested 27 h posttransfection for total Env surface expression and PG16 binding. To measure Env expression, cells were washed with cold PBS-BSA, stained for 40 min with anti-myc Alexa 647 (clone 9B11, 1/200 dilution; Cell Signaling Technology), and washed twice. Cells tested for PG16 binding were washed with cold PBS-BSA, incubated on ice for 1 h with 2 nM PG16, washed twice, incubated on ice for 40 min with APC-conjugated anti-human IgG Fc (clone HP6017, 1/300 dilution; BioLegend), and washed twice. Cells were analyzed on a BD LSR II flow cytometer.

BG505 SOSIP.664 purification. BG505 SOSIP.664 (T332N) was subcloned into pCEP4 (NheI-XhoI sites) with a C-terminal Gly/Ser-rich linker and His_8 tag. Plasmids were transfected into Expi293F cultures using a protocol modified from that of Nguyen et al. (91); per ml of culture, 1 μg of DNA was mixed with 5 μg of linearized polyethyleneimine (MW 25,000; Polysciences) in 100 μl of Opti-MEM (Gibco). The mixture was incubated for 20 min at room temperature and then added to the culture at a density of 2×10^6/ml. Expifectamine transfection enhancers were added 18 h posttransfection. Cells were centrifuged 4 days posttransfection, and secreted protein was purified from the culture supernatant.

Protein was purified at 4°C. The supernatant was dialyzed against 20 mM Tris (pH 8.0)–225 mM NaCl for 6 to 8 h, followed by dialysis overnight against 20 mM Tris (pH 8.0)–20 mM imidazole–300 mM NaCl. Equilibrated Ni-NTA (50% slurry, 500 μl per 40 ml of culture; Thermo Scientific) was incubated with the sample for 1 h on a rocker, collected in a gravity column, and washed with 20 ml of purification buffer (20 mM Tris [pH 8.0], 300 mM NaCl) containing 20 mM imidazole. Protein was eluted using a step gradient of purification buffer containing 50, 100, and 250 mM imidazole (1 ml per fraction). Fractions containing protein were pooled, concentrated using a 30-kDa MWCO centrifugal device (Sartorius) and separated by size exclusion chromatography using a Superose 6 increase 10/300 GL column on an ÄKTA pure system (GE Healthcare) with PBS as the running buffer.

Data availability. Analyzed and raw deep sequencing data have been deposited in NCBI's Gene Expression Omnibus (79) under series accession numbers GSE102276 (BaL gp160), GSE117328 (DU422 gp140), and GSE126136 (001428 Env interactions with MA). The deposits include commands for running Enrich scripts to replicate data analysis, as well as additional details on primer sequences and sort conditions.

Plasmid availability. Plasmids have been deposited with Addgene under ID numbers 100918 to 100933, 111837 to 111847, and 123212 to 123283.

ACKNOWLEDGMENTS

Barbara Pilas, Barbara Balhan, and Angela Kouris at the UIUC Roy J. Carver Biotechnology Center assisted with flow cytometry, and Alvaro Hernandez and Chris Wright helped with deep sequencing.

This study was supported by the National Institute of Allergy and Infectious Diseases of the National Institutes of Health under award R01AI129719. The content is solely the responsibility of the authors and does not necessarily represent the official views of the National Institutes of Health. The University of Illinois has filed a patent with E.P. and J.D.H. as coinventors covering aspects of this work.

Downloaded from https://journals.asm.org/journal/jvi on 24 February 2022 by 65.21.193.86.

REFERENCES

1. Merk A, Subramaniam S. 2013. HIV-1 envelope glycoprotein structure. Curr Opin Struct Biol 23:268–276. https://doi.org/10.1016/j.sbi.2013.03.007.
2. Huang C-C, Lam SN, Acharya P, Tang M, Xiang S-H, Hussan SS-U, Stanfield RL, Robinson J, Sodroski J, Wilson IA, Wyatt R, Bewley CA, Kwong PD. 2007. Structures of the CCR5 N terminus and of a tyrosine-sulfated antibody with HIV-1 gp120 and CD4. Science 317:1930–1934. https://doi.org/10.1126/science.1145373.
3. Wu L, Gerard NP, Wyatt R, Choe H, Parolin C, Ruffing N, Borsetti A, Cardoso AA, Desjardin E, Newman W, Gerard C, Sodroski J. 1996. CD4-induced interaction of primary HIV-1 gp120 glycoproteins with the chemokine receptor CCR-5. Nature 384:179–183. https://doi.org/10.1038/384179a0.
4. Liu J, Bartesaghi A, Borgnia MJ, Sapiro G, Subramaniam S. 2008. Molecular architecture of native HIV-1 gp120 trimers. Nature 455:109–113. https://doi.org/10.1038/nature07159.
5. Burton DR, Ahmed R, Barouch DH, Butera ST, Crotty S, Godzik A, Kaufmann DE, McElrath MJ, Nussenzweig MC, Pulendran B, Scanlan CN, Schief WR, Silvestri G, Streeck H, Walker BD, Walker LM, Ward AB, Wilson IA, Wyatt R. 2012. A blueprint for HIV vaccine discovery. Cell Host Microbe 12:396–407. https://doi.org/10.1016/j.chom.2012.09.008.
6. Moore PL, Crooks ET, Porter L, Zhu P, Cayanan CS, Grise H, Corcoran P, Zwick MB, Franti M, Morris L, Roux KH, Burton DR, Binley JM. 2006. Nature of nonfunctional envelope proteins on the surface of human immunodeficiency virus type 1. J Virol 80:2515–2528. https://doi.org/10.1128/JVI.80.5.2515-2528.2006.
7. Herrera C, Klasse PJ, Michael E, Kake S, Barnes K, Kibler CW, Campbell-Gardener L, Si Z, Sodroski J, Moore JP, Beddows S. 2005. The impact of envelope glycoprotein cleavage on the antigenicity, infectivity, and neutralization sensitivity of Env-pseudotyped human immunodeficiency virus type 1 particles. Virology 338:154–172. https://doi.org/10.1016/j.virol.2005.05.002.
8. Sattentau QJ, Moore JP. 1995. Human immunodeficiency virus type 1 neutralization is determined by epitope exposure on the gp120 oligomer. J Exp Med 182:185–196. https://doi.org/10.1084/jem.182.1.185.
9. Parren PW, Mondor I, Naniche D, Ditzel HJ, Klasse PJ, Burton DR, Sattentau QJ. 1998. Neutralization of human immunodeficiency virus type 1 by antibody to gp120 is determined primarily by occupancy of sites on the virion irrespective of epitope specificity. J Virol 72:3512–3519.
10. Parren PW, Gauduin MC, Koup RA, Poignard P, Fisicaro P, Burton DR, Sattentau QJ. 1997. Relevance of the antibody response against human immunodeficiency virus type 1 envelope to vaccine design. Immunol Lett 57:105–112. https://doi.org/10.1016/S0165-2478(97)00043-6.
11. Sanders RW, Moore JP. 2017. Native-like Env trimers as a platform for HIV-1 vaccine design. Immunol Rev 275:161–182. https://doi.org/10.1111/imr.12481.
12. Ward AB, Wilson IA. 2017. The HIV-1 envelope glycoprotein structure: nailing down a moving target. Immunol Rev 275:21–32. https://doi.org/10.1111/imr.12507.
13. Sanders RW, Vesanen M, Schuelke N, Master A, Schiffner L, Kalyanaraman R, Paluch M, Berkhout B, Maddon PJ, Olson WC, Lu M, Moore JP. 2002. Stabilization of the soluble, cleaved, trimeric form of the envelope glycoprotein complex of human immunodeficiency virus type 1. J Virol 76:8875–8889. https://doi.org/10.1128/JVI.76.17.8875-8889.2002.
14. Binley JM, Sanders RW, Clas B, Schuelke N, Master A, Guo Y, Kajumo F, Anselma DJ, Maddon PJ, Olson WC, Moore JP. 2000. A recombinant human immunodeficiency virus type 1 envelope glycoprotein complex stabilized by an intermolecular disulfide bond between the gp120 and gp41 subunits is an antigenic mimic of the trimeric virion-associated structure. J Virol 74:627–643. https://doi.org/10.1128/JVI.74.2.627-643.2000.
15. Sanders RW, Derking R, Cupo A, Julien J-P, Yasmeen A, de Val N, Kim HJ, Blattner C, la Pena de AT, Korzun J, Golabek M, de Los Reyes K, Ketas TJ, van Gils MJ, King CR, Wilson IA, Ward AB, Klasse PJ, Moore JP. 2013. A next-generation cleaved, soluble HIV-1 Env trimer, BG505 SOSIP.664 gp140, expresses multiple epitopes for broadly neutralizing but not non-neutralizing antibodies. PLoS Pathog 9:e1003618. https://doi.org/10.1371/journal.ppat.1003618.
16. de Taeye SW, Ozorowski G, Torrents de la Peña A, Guttman M, Julien J-P, van den Kerkhof T, Burger JA, Pritchard LK, Pugach P, Yasmeen A, Crampton J, Hu J, Bontjer I, Torres JL, Arendt H, DeStefano J, Koff WC, Schuitemaker H, Eggink D, Berkhout B, Dean H, LaBranche C, Crotty S, Crispin M, Montefiori DC, Klasse PJ, Lee KK, Moore JP, Wilson IA, Ward AB, Sanders RW. 2015. Immunogenicity of stabilized HIV-1 envelope trimers with reduced exposure of non-neutralizing epitopes. Cell 163:1702–1715. https://doi.org/10.1016/j.cell.2015.11.056.
17. Kulp DW, Steichen JM, Pauthner M, Hu X, Schiffner T, Liguori A, Cottrell CA, Havenar-Daughton C, Ozorowski G, Georgeson E, Kalyuzhniy O, Willis JR, Kubitz M, Adachi Y, Reiss SM, Shin M, de Val N, Ward AB, Crotty S, Burton DR, Schief WR. 2017. Structure-based design of native-like HIV-1 envelope trimers to silence non-neutralizing epitopes and eliminate CD4 binding. Nat Commun 8:1655. https://doi.org/10.1038/s41467-017-01549-6.
18. Kwon YD, Pancera M, Acharya P, Georgiev IS, Crooks ET, Gorman J, Joyce MG, Guttman M, Ma X, Narpala S, Soto C, Terry DS, Yang Y, Zhou T, Ahlsen G, Bailer RT, Chambers M, Chuang G-Y, Doria-Rose NA, Druz A, Hallen MA, Harned A, Kirys T, Louder MK, O'Dell S, Ofek G, Osawa K, Prabhakaran M, Sastry M, Stewart-Jones GBE, Stuckey J, Thomas PV, Tittley T, Williams C, Zhang B, Zhao H, Zhou Z, Donald BR, Lee LK, Zolla-Pazner S, Baxa U, Schön A, Freire E, Shapiro L, Lee KK, Arthos J, Munro JB, Blanchard SC, Mothes W, Binley JM, McDermott AB, Mascola JR, Kwong PD. 2015. Crystal structure, conformational fixation and entry-related interactions of mature ligand-free HIV-1 Env. Nat Struct Mol Biol 22:522–531. https://doi.org/10.1038/nsmb.3051.
19. Crooks ET, Tong T, Osawa K, Binley JM. 2011. Enzyme digests eliminate nonfunctional Env from HIV-1 particle surfaces, leaving native Env trimers intact and viral infectivity unaffected. J Virol 85:5825–5839. https://doi.org/10.1128/JVI.00154-11.
20. Fowler DM, Fields S. 2014. Deep mutational scanning: a new style of protein science. Nat Methods 11:801–807. https://doi.org/10.1038/nmeth.3027.
21. Jardine JG, Kulp DW, Havenar-Daughton C, Sarkar A, Briney B, Sok D, Sesterhenn F, Ereño-Orbea J, Kalyuzhniy O, Deresa I, Hu X, Spencer S, Jones M, Georgeson E, Adachi Y, Kubitz M, deCamp AC, Julien J-P, Wilson IA, Burton DR, Crotty S, Schief WR. 2016. HIV-1 broadly neutralizing antibody precursor B cells revealed by germline-targeting immunogen. Science 351:1458–1463. https://doi.org/10.1126/science.aad9195.
22. Steichen JM, Kulp DW, Tokatlian T, Escolano A, Dosenovic P, Stanfield RL, McCoy LE, Ozorowski G, Hu X, Kalyuzhniy O, Briney B, Schiffner T, Garces F, Freund NT, Gitlin AD, Menis S, Georgeson E, Kubitz M, Adachi Y, Jones M, Mutafyan AA, Yun DS, Mayer CT, Ward AB, Burton DR, Wilson IA, Irvine DJ, Nussenzweig MC, Schief WR. 2016. HIV vaccine design to target germline precursors of glycan-dependent broadly neutralizing antibodies. Immunity 45:483–496. https://doi.org/10.1016/j.immuni.2016.08.016.
23. Dingens AS, Haddox HK, Overbaugh J, Bloom JD. 2017. Comprehensive mapping of HIV-1 escape from a broadly neutralizing antibody. Cell Host Microbe 21:777–787. https://doi.org/10.1016/j.chom.2017.05.003.
24. Dingens AS, Acharya P, Haddox HK, Rawi R, Xu K, Chuang G-Y, Wei H, Zhang B, Mascola JR, Carragher B, Potter CS, Overbaugh J, Kwong PD, Bloom JD. 2018. Complete functional mapping of infection- and vaccine-elicited antibodies against the fusion peptide of HIV. PLoS Pathog 14:e1007159. https://doi.org/10.1371/journal.ppat.1007159.
25. Haddox HK, Dingens AS, Bloom JD. 2016. Experimental estimation of the effects of all amino-acid mutations to HIV's envelope protein on viral replication in cell culture. PLoS Pathog 12:e1006114. https://doi.org/10.1371/journal.ppat.1006114.
26. Kovacs JM, Noeldeke E, Ha HJ, Peng H, Rits-Volloch S, Harrison SC, Chen B. 2014. Stable, uncleaved HIV-1 envelope glycoprotein gp140 forms a tightly folded trimer with a native-like structure. Proc Natl Acad Sci U S A 111:18542–18547. https://doi.org/10.1073/pnas.1422269112.
27. Walker LM, Phogat SK, Chan-Hui P-Y, Wagner D, Phung P, Goss JL, Wrin T, Simek MD, Fling S, Mitcham JL, Lehrman JK, Priddy FH, Olsen OA, Frey SM, Hammond PW, Protocol G, Kaminsky S, Zamb T, Moyle M, Koff WC, Poignard P, Burton DR. 2009. Broad and potent neutralizing antibodies from an African donor reveal a new HIV-1 vaccine target. Science 326:285–289. https://doi.org/10.1126/science.1178746.
28. Julien J-P, Lee JH, Cupo A, Murin CD, Derking R, Hoffenberg S, Caulfield MJ, King CR, Marozsan AJ, Klasse PJ, Sanders RW, Moore JP, Wilson IA, Ward AB. 2013. Asymmetric recognition of the HIV-1 trimer by broadly neutralizing antibody PG9. Proc Natl Acad Sci U S A 110:4351–4356. https://doi.org/10.1073/pnas.1217537110.
29. Tran EEH, Borgnia MJ, Kuybeda O, Schauder DM, Bartesaghi A, Frank GA,

Downloaded from https://journals.asm.org/journal/jvi on 24 February 2022 by 65.21.193.86.

Sapiro G, Milne JLS, Subramaniam S. 2012. Structural mechanism of trimeric HIV-1 envelope glycoprotein activation. PLoS Pathog 8:e1002797. https://doi.org/10.1371/journal.ppat.1002797.
30. Li Y, O'Dell S, Walker LM, Wu X, Guenaga J, Feng Y, Schmidt SD, McKee K, Louder MK, Ledgerwood JE, Graham BS, Haynes BF, Burton DR, Wyatt RT, Mascola JR. 2011. Mechanism of neutralization by the broadly neutralizing HIV-1 monoclonal antibody VRC01. J Virol 85:8954–8967. https://doi.org/10.1128/JVI.00754-11.
31. Moore JP, McKeating JA, Weiss RA, Sattentau QJ. 1990. Dissociation of gp120 from HIV-1 virions induced by soluble CD4. Science 250: 1139–1142. https://doi.org/10.1126/science.2251501.
32. Wu X, Yang Z-Y, Li Y, Hogerkorp C-M, Schief WR, Seaman MS, Zhou T, Schmidt SD, Wu L, Xu L, Longo NS, McKee K, O'Dell S, Louder MK, Wycuff DL, Feng Y, Nason M, Doria-Rose N, Connors M, Kwong PD, Roederer M, Wyatt RT, Nabel GJ, Mascola JR. 2010. Rational design of envelope identifies broadly neutralizing human monoclonal antibodies to HIV-1. Science 329:856–861. https://doi.org/10.1126/science.1187659.
33. Seaman MS, Janes H, Hawkins N, Grandpre LE, Devoy C, Giri A, Coffey RT, Harris L, Wood B, Daniels MG, Bhattacharya T, Lapedes A, Polonis VR, McCutchan FE, Gilbert PB, Self SG, Korber BT, Montefiori DC, Mascola JR. 2010. Tiered categorization of a diverse panel of HIV-1 Env pseudoviruses for assessment of neutralizing antibodies. J Virol 84:1439–1452. https://doi.org/10.1128/JVI.02108-09.
34. Heredia JD, Park J, Brubaker RJ, Szymanski SK, Gill KS, Procko E. 2018. Mapping interaction sites on human chemokine receptors by deep mutational scanning. J Immunol 200:3825–3839. https://doi.org/10.4049/jimmunol.1800343.
35. Park J, Selvam B, Sanematsu K, Shigemura N, Shukla D, Procko E. 2019. Structural architecture of a dimeric class C GPCR based on co-trafficking of sweet taste receptor subunits. J Biol Chem 2019: jbc.RA118.006173.
36. Jones DR, Suzuki K, Piller SC. 2002. A 100-amino acid truncation in the cytoplasmic tail of glycoprotein 41 in the reference HIV type 1 strain RF. AIDS Res Hum Retroviruses 18:513–517. https://doi.org/10.1089/088922202317406664.
37. Holtkotte D, Pfeiffer T, Pisch T, Bosch V. 2006. Selection and characterization of a replication-competent human immunodeficiency virus type 1 variant encoding C-terminally truncated env. AIDS Res Hum Retroviruses 22:57–65. https://doi.org/10.1089/aid.2006.22.57.
38. Stano A, Leaman DP, Kim AS, Zhang L, Autin L, Ingale J, Gift SK, Truong J, Wyatt RT, Olson AJ, Zwick MB. 2017. Dense array of spikes on HIV-1 virion particles. J Virol 91:5315.
39. Pancera M, Shahzad-Ul-Hussan S, Doria-Rose NA, McLellan JS, Bailer RT, Dai K, Loesgen S, Louder MK, Staupe RP, Yang Y, Zhang B, Parks R, Eudailey J, Lloyd KE, Blinn J, Alam SM, Haynes BF, Amin MN, Wang L-X, Burton DR, Koff WC, Nabel GJ, Mascola JR, Bewley CA, Kwong PD. 2013. Structural basis for diverse N-glycan recognition by HIV-1-neutralizing V1-V2-directed antibody PG16. Nat Struct Mol Biol 20:804–813. https://doi.org/10.1038/nsmb.2600.
40. Kwong PD, Wyatt R, Robinson J, Sweet RW, Sodroski J, Hendrickson WA. 1998. Structure of an HIV gp120 envelope glycoprotein in complex with the CD4 receptor and a neutralizing human antibody. Nature 393: 648–659. https://doi.org/10.1038/31405.
41. Myszka DG, Sweet RW, Hensley P, Brigham-Burke M, Kwong PD, Hendrickson WA, Wyatt R, Sodroski J, Doyle ML. 2000. Energetics of the HIV gp120-CD4 binding reaction. Proc Natl Acad Sci U S A 97:9026–9031. https://doi.org/10.1073/pnas.97.16.9026.
42. Ozorowski G, Pallesen J, de Val N, Lyumkis D, Cottrell CA, Torres JL, Copps J, Stanfield RL, Cupo A, Pugach P, Moore JP, Wilson IA, Ward AB. 2017. Open and closed structures reveal allostery and pliability in the HIV-1 envelope spike. Nature 547:360–363. https://doi.org/10.1038/nature23010.
43. François KO, Balzarini J. 2011. The highly conserved glycan at asparagine 260 of HIV-1 gp120 is indispensable for viral entry. J Biol Chem 286: 42900–42910. https://doi.org/10.1074/jbc.M111.274456.
44. Wang W, Nie J, Prochnow C, Truong C, Jia Z, Wang S, Chen XS, Wang Y. 2013. A systematic study of the N-glycosylation sites of HIV-1 envelope protein on infectivity and antibody-mediated neutralization. Retrovirology 10:14. https://doi.org/10.1186/1742-4690-10-14.
45. Kong L, Wilson IA, Kwong PD. 2015. Crystal structure of a fully glycosylated HIV-1 gp120 core reveals a stabilizing role for the glycan at Asn262. Proteins 83:590–596. https://doi.org/10.1002/prot.24747.
46. McLellan JS, Pancera M, Carrico C, Gorman J, Julien J-P, Khayat R, Louder R, Pejchal R, Sastry M, Dai K, O'Dell S, Patel N, Shahzad-Ul-Hussan S, Yang Y, Zhang B, Zhou T, Zhu J, Boyington JC, Chuang G-Y, Diwanji D, Georgiev I, Do Kwon Y, Lee D, Louder MK, Moquin S, Schmidt SD, Yang Z-Y, Bonsignori M, Crump JA, Kapiga SH, Sam NE, Haynes BF, Burton DR, Koff WC, Walker LM, Phogat S, Wyatt R, Orwenyo J, Wang L-X, Arthos J, Bewley CA, Mascola JR, Nabel GJ, Schief WR, Ward AB, Wilson IA, Kwong PD. 2011. Structure of HIV-1 gp120 V1/V2 domain with broadly neutralizing antibody PG9. Nature 480:336–343. https://doi.org/10.1038/nature10696.
47. Chuang G-Y, Geng H, Pancera M, Xu K, Cheng C, Acharya P, Chambers M, Druz A, Tsybovsky Y, Wanninger TG, Yang Y, Doria-Rose NA, Georgiev IS, Gorman J, Joyce MG, O'Dell S, Zhou T, McDermott AB, Mascola JR, Kwong PD. 2017. Structure-based design of a soluble prefusion-closed HIV-1 Env trimer with reduced CD4 affinity and improved immunogenicity. J Virol 91:542.
48. Lee JH, Andrabi R, Su C-Y, Yasmeen A, Julien J-P, Kong L, Wu NC, McBride R, Sok D, Pauthner M, Cottrell CA, Nieusma T, Blattner C, Paulson JC, Klasse PJ, Wilson IA, Burton DR, Ward AB. 2017. A broadly neutralizing antibody targets the dynamic HIV envelope trimer apex via a long, rigidified, and anionic β-hairpin structure. Immunity 46:690–702. https://doi.org/10.1016/j.immuni.2017.03.017.
49. Grupping K, Selhorst P, Michiels J, Vereecken K, Heyndrickx L, Kessler P, Vanham G, Martin L, Ariën KK. 2012. MiniCD4 protein resistance mutations affect binding to the HIV-1 gp120 CD4 binding site and decrease entry efficiency. Retrovirology 9:36. https://doi.org/10.1186/1742-4690-9-36.
50. Lee JH, de Val N, Lyumkis D, Ward AB. 2015. Model building and refinement of a natively glycosylated HIV-1 Env protein by high-resolution cryoelectron microscopy. Structure 23:1943–1951. https://doi.org/10.1016/j.str.2015.07.020.
51. Mouquet H, Scharf L, Euler Z, Liu Y, Eden C, Scheid JF, Halper-Stromberg A, Gnanapragasam PNP, Spencer DIR, Seaman MS, Schuitemaker H, Feizi T, Nussenzweig MC, Bjorkman PJ. 2012. Complex-type N-glycan recognition by potent broadly neutralizing HIV antibodies. Proc Natl Acad Sci U S A 109:E3268–E3277. https://doi.org/10.1073/pnas.1217207109.
52. Garces F, Sok D, Kong L, McBride R, Kim HJ, Saye-Francisco KF, Julien J-P, Hua Y, Cupo A, Moore JP, Paulson JC, Ward AB, Burton DR, Wilson IA. 2014. Structural evolution of glycan recognition by a family of potent HIV antibodies. Cell 159:69–79. https://doi.org/10.1016/j.cell.2014.09.009.
53. Julien J-P, Sok D, Khayat R, Lee JH, Doores KJ, Walker LM, Ramos A, Diwanji DC, Pejchal R, Cupo A, Katpally U, Depetris RS, Stanfield RL, McBride R, Marozsan AJ, Paulson JC, Sanders RW, Moore JP, Burton DR, Poignard P, Ward AB, Wilson IA. 2013. Broadly neutralizing antibody PGT121 allosterically modulates CD4 binding via recognition of the HIV-1 gp120 V3 base and multiple surrounding glycans. PLoS Pathog 9:e1003342. https://doi.org/10.1371/journal.ppat.1003342.
54. Postler TS, Desrosiers RC. 2013. The tale of the long tail: the cytoplasmic domain of HIV-1 gp41. J Virol 87:2–15. https://doi.org/10.1128/JVI.02053-12.
55. Jeffs SA, Goriup S, Kebble B, Crane D, Bolgiano B, Sattentau Q, Jones S, Holmes H. 2004. Expression and characterization of recombinant oligomeric envelope glycoproteins derived from primary isolates of HIV-1. Vaccine 22:1032–1046. https://doi.org/10.1016/j.vaccine.2003.08.042.
56. Go EP, Cupo A, Ringe R, Pugach P, Moore JP, Desaire H. 2015. Native conformation and canonical disulfide bond formation are interlinked properties of HIV-1 Env glycoproteins. J Virol 90:2884–2894. https://doi.org/10.1128/JVI.01953-15.
57. Wu S-R, Löving R, Lindqvist B, Hebert H, Koeck PJB, Sjöberg M, Garoff H. 2010. Single-particle cryoelectron microscopy analysis reveals the HIV-1 spike as a tripod structure. Proc Natl Acad Sci U S A 107:18844–18849. https://doi.org/10.1073/pnas.1007227107.
58. White TA, Bartesaghi A, Borgnia MJ, Meyerson JR, la Cruz de MJV, Bess JW, Nandwani R, Hoxie JA, Lifson JD, Milne JLS, Subramaniam S. 2010. Molecular architectures of trimeric SIV and HIV-1 envelope glycoproteins on intact viruses: strain-dependent variation in quaternary structure. PLoS Pathog 6:e1001249. https://doi.org/10.1371/journal.ppat.1001249.
59. Julien J-P, Cupo A, Sok D, Stanfield RL, Lyumkis D, Deller MC, Klasse PJ, Burton DR, Sanders RW, Moore JP, Ward AB, Wilson IA. 2013. Crystal structure of a soluble cleaved HIV-1 envelope trimer. Science 342: 1477–1483. https://doi.org/10.1126/science.1245625.
60. Lyumkis D, Julien J-P, de Val N, Cupo A, Potter CS, Klasse PJ, Burton DR, Sanders RW, Moore JP, Carragher B, Wilson IA, Ward AB. 2013. Cryo-EM structure of a fully glycosylated soluble cleaved HIV-1 envelope trimer. Science 342:1484–1490. https://doi.org/10.1126/science.1245627.

Downloaded from https://journals.asm.org/journal/jvi on 24 February 2022 by 65.21.193.86.

61. Mao Y, Wang L, Gu C, Herschhorn A, Xiang S-H, Haim H, Yang X, Sodroski J. 2012. Subunit organization of the membrane-bound HIV-1 envelope glycoprotein trimer. Nat Struct Mol Biol 19:893–899. https://doi.org/10.1038/nsmb.2351.
62. Pancera M, Zhou T, Druz A, Georgiev IS, Soto C, Gorman J, Huang J, Acharya P, Chuang G-Y, Ofek G, Stewart-Jones GBE, Stuckey J, Bailer RT, Joyce MG, Louder MK, Tumba N, Yang Y, Zhang B, Cohen MS, Haynes BF, Mascola JR, Morris L, Munro JB, Blanchard SC, Mothes W, Connors M, Kwong PD. 2014. Structure and immune recognition of trimeric pre-fusion HIV-1 Env. Nature 514:455–461. https://doi.org/10.1038/nature13808.
63. Montefiori DC, Roederer M, Morris L, Seaman MS. 2018. Neutralization tiers of HIV-1. Curr Opin HIV AIDS 13:128–136. https://doi.org/10.1097/COH.0000000000000442.
64. Ringe RP, Sanders RW, Yasmeen A, Kim HJ, Lee JH, Cupo A, Korzun J, Derking R, van Montfort T, Julien J-P, Wilson IA, Klasse PJ, Ward AB, Moore JP. 2013. Cleavage strongly influences whether soluble HIV-1 envelope glycoprotein trimers adopt a native-like conformation. Proc Natl Acad Sci U S A 110:18256–18261. https://doi.org/10.1073/pnas.1314351110.
65. Torrents de la Peña A, Julien J-P, de Taeye SW, Garces F, Guttman M, Ozorowski G, Pritchard LK, Behrens A-J, Go EP, Burger JA, Schermer EE, Sliepen K, Ketas TJ, Pugach P, Yasmeen A, Cottrell CA, Torres JL, Vavourakis CD, van Gils MJ, LaBranche C, Montefiori DC, Desaire H, Crispin M, Klasse PJ, Lee KK, Moore JP, Ward AB, Wilson IA, Sanders RW. 2017. Improving the immunogenicity of native-like HIV-1 envelope trimers by hyperstabilization. Cell Rep 20:1805–1817. https://doi.org/10.1016/j.celrep.2017.07.077.
66. Huang J, Kang BH, Pancera M, Lee JH, Tong T, Feng Y, Imamichi H, Georgiev IS, Chuang G-Y, Druz A, Doria-Rose NA, Laub L, Sliepen K, van Gils MJ, la Pena de AT, Derking R, Klasse PJ, Migueles SA, Bailer RT, Alam M, Pugach P, Haynes BF, Wyatt RT, Sanders RW, Binley JM, Ward AB, Mascola JR, Kwong PD, Connors M. 2014. Broad and potent HIV-1 neutralization by a human antibody that binds the gp41-gp120 interface. Nature 515:138–142. https://doi.org/10.1038/nature13601.
67. Muranyi W, Malkusch S, Müller B, Heilemann M, Kräusslich H-G. 2013. Super-resolution microscopy reveals specific recruitment of HIV-1 envelope proteins to viral assembly sites dependent on the envelope C-terminal tail. PLoS Pathog 9:e1003198. https://doi.org/10.1371/journal.ppat.1003198.
68. Hermida-Matsumoto L, Resh MD. 2000. Localization of human immunodeficiency virus type 1 Gag and Env at the plasma membrane by confocal imaging. J Virol 74:8670–8679. https://doi.org/10.1128/JVI.74.18.8670-8679.2000.
69. Tedbury PR, Freed EO. 2014. The role of matrix in HIV-1 envelope glycoprotein incorporation. Trends Microbiol 22:372–378. https://doi.org/10.1016/j.tim.2014.04.012.
70. Freed EO, Martin MA. 1996. Domains of the human immunodeficiency virus type 1 matrix and gp41 cytoplasmic tail required for envelope incorporation into virions. J Virol 70:341–351.
71. Freed EO, Martin MA. 1995. Virion incorporation of envelope glycoproteins with long but not short cytoplasmic tails is blocked by specific, single amino acid substitutions in the human immunodeficiency virus type 1 matrix. J Virol 69:1984–1989.
72. Brandano L, Stevenson M. 2012. A highly conserved residue in the C-terminal helix of HIV-1 matrix is required for envelope incorporation into virus particles. J Virol 86:2347–2359. https://doi.org/10.1128/JVI.06047-11.
73. Ghanam RH, Samal AB, Fernandez TF, Saad JS. 2012. Role of the HIV-1 matrix protein in Gag intracellular trafficking and targeting to the plasma membrane for virus assembly. Front Microbiol 3:55. https://doi.org/10.3389/fmicb.2012.00055.
74. Kodama Y, Hu C-D. 2010. An improved bimolecular fluorescence complementation assay with a high signal-to-noise ratio. Biotechniques 49:793–805. https://doi.org/10.2144/000113519.
75. Hu C-D, Chinenov Y, Kerppola TK. 2002. Visualization of interactions among bZIP and Rel family proteins in living cells using bimolecular fluorescence complementation. Mol Cell 9:789–798. https://doi.org/10.1016/S1097-2765(02)00496-3.
76. Murakami T, Freed EO. 2000. The long cytoplasmic tail of gp41 is required in a cell type-dependent manner for HIV-1 envelope glycoprotein incorporation into virions. Proc Natl Acad Sci USA 97:343–348. https://doi.org/10.1073/pnas.97.1.343.
77. Tedbury PR, Novikova M, Ablan SD, Freed EO. 2016. Biochemical evidence of a role for matrix trimerization in HIV-1 envelope glycoprotein incorporation. Proc Natl Acad Sci U S A 113:E182–E190. https://doi.org/10.1073/pnas.1516618113.
78. Procko E, Hedman R, Hamilton K, Seetharaman J, Fleishman SJ, Su M, Aramini J, Kornhaber G, Hunt JF, Tong L, Montelione GT, Baker D. 2013. Computational design of a protein-based enzyme inhibitor. J Mol Biol 425:3563–3575. https://doi.org/10.1016/j.jmb.2013.06.035.
79. Edgar R, Domrachev M, Lash AE. 2002. Gene Expression Omnibus: NCBI gene expression and hybridization array data repository. Nucleic Acids Res 30:207–210. https://doi.org/10.1093/nar/30.1.207.
80. Fowler DM, Araya CL, Gerard W, Fields S. 2011. Enrich: software for analysis of protein function by enrichment and depletion of variants. Bioinformatics 27:3430–3431. https://doi.org/10.1093/bioinformatics/btr577.
81. Kwong PD, Doyle ML, Casper DJ, Cicala C, Leavitt SA, Majeed S, Steenbeke TD, Venturi M, Chaiken I, Fung M, Katinger H, Parren PWIH, Robinson J, Van Ryk D, Wang L, Burton DR, Freire E, Wyatt R, Sodroski J, Hendrickson WA, Arthos J. 2002. HIV-1 evades antibody-mediated neutralization through conformational masking of receptor-binding sites. Nature 420:678–682. https://doi.org/10.1038/nature01188.
82. Pantophlet R, Wilson IA, Burton DR. 2004. Improved design of an antigen with enhanced specificity for the broadly HIV-neutralizing antibody b12. Protein Eng Des Sel 17:749–758. https://doi.org/10.1093/protein/gzh085.
83. Gorny MK, Xu JY, Gianakakos V, Karwowska S, Williams C, Sheppard HW, Hanson CV, Zolla-Pazner S. 1991. Production of site-selected neutralizing human monoclonal antibodies against the third variable domain of the human immunodeficiency virus type 1 envelope glycoprotein. Proc Natl Acad Sci U S A 88:3238–3242. https://doi.org/10.1073/pnas.88.8.3238.
84. Gorny MK, Williams C, Volsky B, Revesz K, Cohen S, Polonis VR, Honnen WJ, Kayman SC, Krachmarov C, Pinter A, Zolla-Pazner S. 2002. Human monoclonal antibodies specific for conformation-sensitive epitopes of V3 neutralize human immunodeficiency virus type 1 primary isolates from various clades. J Virol 76:9035–9045. https://doi.org/10.1128/JVI.76.18.9035-9045.2002.
85. Gorny MK, Williams C, Volsky B, Revesz K, Wang X-H, Burda S, Kimura T, Konings FAJ, Nádas A, Anyangwe CA, Nyambi P, Krachmarov C, Pinter A, Zolla-Pazner S. 2006. Cross-clade neutralizing activity of human anti-V3 monoclonal antibodies derived from the cells of individuals infected with non-B clades of human immunodeficiency virus type 1. J Virol 80:6865–6872. https://doi.org/10.1128/JVI.02202-05.
86. Hioe CE, Wrin T, Seaman MS, Yu X, Wood B, Self S, Williams C, Gorny MK, Zolla-Pazner S. 2010. Anti-V3 monoclonal antibodies display broad neutralizing activities against multiple HIV-1 subtypes. PLoS One 5:e10254. https://doi.org/10.1371/journal.pone.0010254.
87. Walker LM, Huber M, Doores KJ, Falkowska E, Pejchal R, Julien J-P, Wang S-K, Ramos A, Chan-Hui P-Y, Moyle M, Mitcham JL, Hammond PW, Olsen OA, Phung P, Fling S, Wong C-H, Phogat S, Wrin T, Simek MD, Principal Investigators PG, Koff WC, Wilson IA, Burton DR, Poignard P. 2011. Broad neutralization coverage of HIV by multiple highly potent antibodies. Nature 477:466–470. https://doi.org/10.1038/nature10373.
88. Stewart-Jones GBE, Soto C, Lemmin T, Chuang G-Y, Druz A, Kong R, Thomas PV, Wagh K, Zhou T, Behrens A-J, Bylund T, Choi CW, Davison JR, Georgiev IS, Joyce MG, Kwon YD, Pancera M, Taft J, Yang Y, Zhang B, Shivatare SS, Shivatare VS, Lee C-C, Wu C-Y, Bewley CA, Burton DR, Koff WC, Connors M, Crispin M, Baxa U, Korber BT, Wong C-H, Mascola JR, Kwong PD. 2016. Trimeric HIV-1-Env structures define glycan shields from clades A, B, and G. Cell 165:813–826. https://doi.org/10.1016/j.cell.2016.04.010.
89. Cooper S, Khatib F, Treuille A, Barbero J, Lee J, Beenen M, Leaver-Fay A, Baker D, Popović Z, Players F. 2010. Predicting protein structures with a multiplayer online game. Nature 466:756–760. https://doi.org/10.1038/nature09304.
90. Leaver-Fay A, Tyka M, Lewis SM, Lange OF, Thompson J, Jacak R, Kaufman K, Renfrew PD, Smith CA, Sheffler W, Davis IW, Cooper S, Treuille A, Mandell DJ, Richter F, Ban Y-E, Fleishman SJ, Corn JE, Kim DE, Lyskov S, Berrondo M, Mentzer S, Popović Z, Havranek JJ, Karanicolas J, Das R, Meiler J, Kortemme T, Gray JJ, Kuhlman B, Baker D, Bradley P. 2011. ROSETTA3: an object-oriented software suite for the simulation and design of macromolecules. Methods Enzymol 487:545–574. https://doi.org/10.1016/B978-0-12-381270-4.00019-6.
91. Nguyen TA, Jo MH, Choi Y-G, Park J, Kwon SC, Hohng S, Kim VN, Woo J-S. 2015. Functional anatomy of the human microprocessor. Cell 161:1374–1387. https://doi.org/10.1016/j.cell.2015.05.010.

Downloaded from https://journals.asm.org/journal/jvi on 24 February 2022 by 65.21.193.86.